This manuscript was accepted for publication to Canadian Journal of Earth Sciences as of January 30, 2025. This accepted version of the manuscript has slightly different and improved content than the original posted version and is the preferred manuscript. Constructive feedback is welcome.

Carbonated Mantle Lithosphere from the Western Canadian Cordillera

Nils Peterson[1,2]

Natasha Barrett[3]

and

James K. Russell[2]

Canadian Journal of Earth Sciences

[1] Galore Creek Mining Corporation, Vancouver, BC Canada.

[2]Volcanology & Petrology Laboratory, Earth Ocean & Atmospheric Science, University of British Columbia, Vancouver, BC Canada.

[3]Mineral Deposit Research Unit, Earth Ocean & Atmospheric Science, University of British Columbia, Vancouver, BC Canada.

*Corresponding Author:

J.K. Russell (krussell@eoas.ubc.ca)

ABSTRACT

Carbonated mantle is a significant source for many alkaline magmas, yet carbonate minerals are rarely preserved in samples of mantle lithosphere. Here, we report the first occurrence of mantle-equilibrated ("primary") carbonate within spinel peridotite xenoliths from the Pacific Coast Ranges of North America. The xenoliths are hosted in a 19 Ma basanite dyke at Mt. Preston, British Columbia near the boundary between the Intermontane and Coast Belts of the Canadian Cordillera. Magnesian calcite (X_{Ca} ~0.90) occurs in all samples as: i) intergranular grains in textural equilibrium with surrounding minerals, ii) inclusions within mantle silicates; and as iii) intergranular or fracture-filling veins. Sulphides (pentlandite and chalcopyrite) occur in association with carbonate. Two-pyroxene geothermometry on carbonate-bearing mantle xenoliths return temperatures of ~815 to 1120 °C, corresponding to depths of ~32 to 55 km on a model geotherm for warm, thin Cordillera-style lithosphere. C–O isotopic compositions of the xenoliths vary as $\delta^{13}C$ = -3 to -6 ‰, and $\delta^{18}O$ = 10 to 12 ‰. Collectively, the textural, geochemical and isotopic evidence suggest that a carbonate melt with associated monosulphide solution metasomatized and enriched previously depleted mantle lithosphere. The metasomatic fluids sourced from the subduction of oceanic crust beneath North America during Coast Plutonic Belt magmatism when Mt. Preston was in an arc to back arc position. The host basanite dyke contains magmatic groundmass calcite ($\delta^{18}O$ = 14±0.2‰, $\delta^{13}C$ = -4±0.2‰, $^{87}Sr/^{86}Sr$ = 0.704018) indicating a high intrinsic P_{CO2} that inhibited thermal decomposition of mantle carbonate within the xenoliths during ascent.

Keywords: Mantle-lithosphere, xenolith, dyke, peridotite, carbonate, sulphide, basanite, metasomatism.

1. Introduction

Mantle-derived xenoliths are commonly sampled and transported to the surface in mafic alkaline magmas and represent direct samples of the Earth's lithospheric mantle (Pearson et al., 2003; Russell and Jones, 2023 and references therein). Beneath mobile belts such as the Canadian Cordillera the mantle lithosphere is relatively thin (<35 km) and warm (800–1200 ^{o}C; Hyndman, 2017 and references therein) and dominated by spinel peridotite. In addition to the major mineral phases, the mantle lithosphere can host accessory minerals including amphiboles (e.g., Ghent et al., 2019), apatite, phlogopite (e.g., Canil and Scarfe, 1989), sulphides (e.g., Delpech et al., 2012; Rielli et al., 2022), and carbonates (Yaxley et al., 1991; Ionov et al., 1996; Rudnick et al., 1993; Ducea et al., 2005). These accessory phases can be important indicators of past metasomatic events (i.e., pervasive fluid or melt enrichment) that influence the mantle solidus, and hence, control mantle melting (e.g., Francis and Ludden, 1995; Laurora et al., 2001). Such phases have also been used to estimate mantle volatile budgets and to inform on the transport and mobilization of metals within the mantle lithosphere (e.g., Rielli et al., 2022; Blanks et al. 2020).

Primary (i.e. mantle-equilibrated) carbonate is stable under typical upper mantle redox conditions, however, is rarely preserved due to rapid decarbonation during xenolith entrainment and transport of carbonated peridotite (e.g., Canil, 1990). Nevertheless, primary carbonate has been reported for mantle xenolith suites deriving from a variety of tectonic settings including active or paleo-subduction zones (e.g., Laurora et al., 2001; Demény et al., 2004; Ducea et al., 2005), intraplate settings (e.g., Moine et al., 2004) and rift margins (e.g. Lee et al., 2000; Perkins et al., 2006). Most primary carbonates are considered to result from enrichment events shortly before eruption, due to features indicative of textural/chemical disequilibrium (e.g., Lee et al., 2000; Demény et al., 2004; Moine et al., 2004; Ducea et al., 2005; Ionov et al., 2006). Even where xenolith-hosed carbonate has been shown to be chemically and isotopically equilibrated with mantle (e.g., Ionov et al., 1996; Yaxley et al., 1998), original textures are rarely preserved and have been modified during magma transport.

Here, we report on a new suite of lithospheric mantle xenoliths preserved in a mafic alkaline dyke exposed at Mt. Preston in western British Columbia (BC; Fig. 1) and described by Peterson et al. (2006) and Peterson (2010). This occurrence is distinguished, relative to

others in the Canadian Cordillera, because it is located at the westernmost margin of the Intermontane Belt, close to the Coast Belt margin (e.g., Wheeler et al., 1991; Fig. 1). These mantle xenoliths, therefore, inform on the thermal and compositional state of the mantle lithosphere underlying this under-represented portion of the Canadian Cordillera. Furthermore, these xenoliths are unique because they preserve mantle-equilibrated (i.e. primary) carbonate in textural and chemical equilibrium. The suite of peridotite xenoliths provides direct evidence for, and the origins of, carbonate-melt metasomatism of the mantle lithosphere underlying this region of the Canadian Cordillera.

2. Geological Setting

2.1. Tectonic Framework

The Canadian Cordillera is an amalgamation of terranes accreted onto the western margin of North American during Middle Jurassic (~185 Ma) to Late Cretaceous (90 to 85 Ma, Insular Belt rocks) time (Monger et al., 1982; Gehrels et al., 2009). The terranes comprising the Intermontane Belt have been interpreted as related fragments of a late Paleozoic to early Mesozoic island arc (Stikine and Quesnel terranes), and its associated accretionary complex (Cache Creek terrane). The Intermontane Belt is separated from the Insular Belt to the west by the Coast Belt, comprising the Coast Mountains Batholith (or Coast Plutonic Complex), the roots of a Middle Jurassic to Eocene magmatic arc (van der Heyden, 1992; Monger et al., 1994; Gehrels et al., 2009), and related rocks (Fig. 1).

Mafic volcanic centers are ubiquitous in the Canadian Cordillera, and they commonly sample the lithosphere underlying their eruptive localities (e.g., Edwards and Russell, 2000; Canil and Hyndman 2023; and references therein). Collections of xenoliths from these occurrences have supported numerous studies of the Cordillera's mantle lithosphere (e.g., Canil and Scarfe, 1989; Peslier et al., 2000; Peslier et al., 2002; Harder and Russell, 2006; Francis et al., 2010 and references therein). Most evidence for metasomatic events within the mantle lithosphere underlying the Canadian Cordillera is indirect (i.e. cryptic metasomatism) and based on geochemical compositions of peridotite xenoliths (e.g., Francis and Ludden, 1995; Peslier et al., 2002). Rare direct evidence for mantle metasomatic events within the

115 Cordilleran mantle derives from the presence of accessory phlogopite (Canil and Scarfe,
116 1989) or pargasitic amphibole (Ghent et al., 2019) within peridotite xenoliths.
117
118 2.2. Host Dyke
119 A xenolith-bearing dyke outcrops on a ridge ~3 km southeast of Mt. Preston at 53°
120 13' 3" N, 126° 41' 58" W (Fig. 1). The near-vertical dyke strikes 145° and is exposed at the
121 ridge crestline where it can be traced continuously down a steep south-facing slope for ~110
122 m (Fig. 2) and several hundred metres further on an inaccessible vertical face. Contacts with
123 the wall rocks are sharp and the dyke varies in thickness from ~1 to 2 m where both contacts
124 are visible; downslope the dyke is as wide as 7 m.
125 The dyke is aphyric, holocrystalline, moderately vesicular (5–30%) and features an
126 aphanitic groundmass (Fig. 2). The groundmass mineralogy comprises ~40 vol.% plagioclase,
127 ~25 % olivine (≤0.5 mm), ~35 % clinopyroxene (≤0.2 mm), and ~3 % of ≤ 0.1 mm subhedral
128 to anhedral crystals of ulvöspinel. Magmatic carbonate, identified as near end-member
129 calcite, occurs as ≤0.5 mm laths and patches in the groundmass, and as larger subhedral grains
130 (≤1 mm) filling or lining vesicles (Fig. 2D–E). Other minor phases include alkali feldspar,
131 nepheline, and apatite.
132 Major element compositions and trace and rare earth element contents of the mafic
133 dyke are reported in Supplementary materials (Table S1). Chemically the dyke is a basanite,
134 has an SiO_2 content of ~43-45 wt.%, an Mg# of 62, and contains 5 wt.% normative nepheline.
135 The basanite has a calculated liquidus of ~1250–1300 °C (MELTS modeling; 15 kbar, QFM,
136 0–1 wt.% H_2O; Asimow and Ghiorso, 1998). A single sample of the dyke was dated by
137 $^{40}Ar/^{39}Ar$ methods and returned a plateau age of 18.72 ± 0.26 Ma (± 2σ) representing a
138 Neogene (early Miocene) crystallization age (see Supplementary Material S2).
139
140 2.3. Xenolith Occurrence
141 Mantle-derived peridotitic xenoliths are especially abundant in the outcrops situated
142 4–8 m below the ridge crest where the dyke narrows to ~1–1.5 m in width (Fig. 2A, B). At
143 this location the xenoliths constitute 50–80 % of the dyke and are concentrated enough to be
144 locally clast-supported (Fig. 2B). The mean diameter of xenoliths at this locality is ~15 cm

and the largest xenolith measured was ~40–50 cm in diameter. Over 150 xenoliths were collected from the dyke and a representative group of 51 xenoliths studied in detail. The peridotite xenoliths are dominated by lherzolite, well-preserved, and show no signs of reacting with the host magma even though several peridotite blocks are crosscut by one or more thin (1–5 mm) planar veins of melt. Xenolith angularity crudely correlates inversely with size. Xenocrysts (2–5 mm) of olivine and pyroxene are rare (< 1%) but ubiquitous within the dyke and presumed to derive from the mechanical breakdown of peridotite xenoliths.

2.4. Dyke Wall Rock

The Mt. Preston region is underlain by Early to Middle Jurassic Hazelton Group rocks, comprising metamorphosed volcanic to volcaniclastic and mudstone-dominated sedimentary rocks (Gordee et al., 2005; Mahoney et al., 2005). The wall rocks to the dyke comprise volcaniclastics that are trachyandesitic to dacitic in composition based on major element chemistry. Regionally, Hazelton rocks are intruded by post-ca. 136 Ma, metamorphosed mafic to intermediate dykes (Gordee et al., 2005). A trachybasalt dyke located within 10 m of the xenolith-bearing dyke of interest representing one of these older intrusions was dated ($^{40}Ar/^{39}Ar$) as 87.74 ± 0.71 Ma (± 2s). There are no carbonate-rich lithologies noted or previously mapped in the region of Mt. Preston.

3. Methods

3.1. Bulk Geochemistry

Samples were prepared for bulk geochemical analysis at the UBC Department of Earth and Ocean Sciences using a jaw crusher followed by pulverization in a tungsten carbide ring mill and then sieved to a grain size of <0.42mm. Analysis of powders for major and trace elements, ferrous iron, H_2O, and CO_2 was carried out at the Geochemical Laboratories, McGill University, Montreal. Major elements were analyzed by X-ray fluorescence (XRF) on fused beads from ignited samples; trace elements were analyzed for using pressed powder pellets. XRF analysis was done on a Philips PW2440 spectrometer. Total iron was determined by XRF, and FeO content was determined by volumetric analysis (ammonium metavanadate titration). Samples were analyzed for CO_2 on an ELTRA CS-800

carbon/sulphur infrared (IR) analyzer. H_2O+ (structurally bonded water) was determined by difference using loss on ignition (LOI), CO_2, SO_3, halogens, and FeO analyses.

3.2. Mineral Compositions

Mineral compositions were measured on a fully automated CAMECA SX-50 electron microprobe at the University of British Columbia, Department of Earth and Ocean Sciences. Operating conditions in wavelength-dispersion mode included: excitation voltage of 15 kV, beam current of 20 nA, 20 s peak count time, 10 s background count time, and a beam diameter of 5 μm (see also Harder and Russell, 2006; Peterson, 2010, p. 152). For carbonate, a beam current of 10 nA and a spot diameter of 10 μm was used. Data reduction was completed using the 'PAP' $\phi(\rho Z)$ method (Pouchou and Pichoir, 1985). Criteria for exclusion of analysis points included low or high totals (<98 or >102 %) or poor totals of oxygen relative to the cation sums. For example, analyses were excluded if the oxygen sum was <5.95 or >6 for pyroxenes normalized based on 4 cations. For geothermometry purposes (see below), at least 8 coexisting clinopyroxene and orthopyroxene grains were analyzed in each xenolith (Full data set in Supplementary Material, Table S6a). These mineral pair compositions were measured on shared grain boundaries within ~20 μm of the grain edges; no zoning was observed in these phases.

3.3. Stable Isotopes

Oxygen, carbon, and strontium isotopic analyses on carbonates were performed on leachates of bulk-rock powders (like other mantle-derived carbonate studies, e.g. Ionov et al. 1993), and in the case of dyke and country rock, also from tungsten carbide microdrilling of carbonate-rich patches. All powdered samples were analyzed at the PCIGR, University of British Columbia, in a Finnigan Delta XL Plus mass spectrometer, using a gas bench with A200 S autosampler.

Oxygen and strontium isotopic compositions of the silicate fraction of the basanite dyke were determined after removal of carbonate from the bulk-rock powders. Powders were immersed in 10% hydrochloric acid, agitated in an ultrasonic bath for 10 minutes, then separated from the leachate via centrifuge. The leaching process was verified by X-ray diffraction. Sample analysis was performed at the Facility for Isotope Research at Queen's

University, Kingston, Ontario. Analysis followed the BrF5 method of Clinton and Mayeda (1963), on a Finnegan MAT 252 mass spectrometer.

4. Xenolith Petrography

4.1. Peridotite Xenoliths

Of the 51 xenoliths studied in detail, 48 have a common assemblage of olivine (ol), clinopyroxene (cpx), orthopyroxene (opx) and spinel (spl). The other samples include two websterites lacking olivine and containing spinel and plagioclase (NP-MP05-69, -96), and a dunite lacking orthopyroxene (NP-MP05-150). Dunites are a minor but common component in Cordilleran suites. The Mt. Preston suite is unimodal (i.e., lherzolite-dominated) based on the definition of Shi et al. (1998) and, in that regard, similar to most other xenolith suites in the Canadian Cordillera. Bimodal suites (i.e., enriched in harzburgite) are found in northwestern BC and southern Yukon (Shi et al., 1998; Francis et al., 2010).

Individual xenoliths exhibit granular textures and show substantial grain size variations (~0.5–2 mm) but rarely contain megacrysts (outsized grains). About a third of the xenoliths show weak to moderate planar fabrics (i.e., mineralogical banding or mineral foliation) at the hand-sample scale. Foliation tends to be stronger (or more easily observed) in fine-grained samples and is weaker in samples with increasing median grain size. Banding is observed as 1–3 mm wide bands of spinel, repeating on a 1 cm scale, or 2–3 mm wide indistinct bands of clinopyroxene, repeating on an approximately 1–2 cm scale. Larger scale segregations, or possibly bands of olivine and clinopyroxene (~1 cm width or greater) also occur.

A few samples contain pyroxene grains featuring reaction zones at their margins where they are in contact with thin veinlets of basanite. Less commonly pyroxene grains show disequilibrium textures on their margins (i.e. Fig. 3E) where they are close to intergranular carbonate grains or carbonate veins. Nonetheless the geothermometry for these rare samples returned internally consistent results based on multiple pairs of pyroxene grains (see below). These textures are not pervasive and likely due to the thermal disturbance and heating of the xenolith during transport. We have only used data from xenoliths for which

the geothermometry results are consistent between multiple pairs of pyroxene grains.

4.2. Carbonate Petrography

We investigated the presence of accessory carbonate in mantle xenoliths using a Cambridge Image Technology™ CL8200 Mk4 cold cathodoluminescence (CL) system attached to a petrographic microscope at the University of British Columbia. Operating conditions included an excitation voltage of 15 kV and a current of 350 μA. Granular carbonate (intergranular or inclusions; Fig. 3A) and/or carbonate veins are found as an accessory phase in all mantle xenoliths and are commonly associated with pentlandite and chalcopyrite (Fig. 3). A single rutile grain was found included in one calcite grain. No hydrous minerals, nor interstitial glass indicative of disequilibrium, were observed. We also used CL to test for the presence of carbonate in two additional crustal xenoliths from the same dyke and mantle xenoliths from two other localities in the Canadian Cordillera. CL examination of these samples found no carbonate. The xenolith-hosted intergranular carbonate is found as discrete ≤0.4 mm grains exhibiting uniform extinction, or as patches with distinct internal crystallographic subdomains (Fig. 3A). The xenolith-hosted carbonate is Mg-bearing ("magnesian") calcite (X_{Ca} of 86–94; see Supplementary Material, Table S6b).

Texturally the intergranular carbonate appears to be in equilibrium with coexisting silicate phases, as suggested by shared triple-point grain boundaries (Fig. 3A–F). Some intergranular carbonate shows concentric zones of Mg-enrichment. Carbonate also occurs as ≤0.2 mm inclusions (Fig. 3H & 3I) in other mantle minerals. Carbonate veins (≤0.1 mm wide) appear as intergranular and crosscutting features (Fig. 3G); some carbonate veins merge with larger grains of carbonate (Fig. 3). Rare, thin veinlets of basanite crosscut all features including carbonate veins, indicating that the carbonate predates entrainment by the basanite magma and, thus, are a mantle feature.

4.3. Sulphide Petrography

Pentlandite and chalcopyrite (≤0.1 mm) were noted in eight of the xenoliths examined by CL and have modal abundances < 1 %. They occur at the edges of carbonate grains (Fig.

3A–C) in contact with silicates, at the margins of carbonate veins, and in inclusion trails with or without associated carbonate.

5. Geochemistry

5.1. Major and Trace Element Geochemistry

Bulk major element compositions of mantle xenoliths have Mg# of 87 to 91, Al_2O_3 contents of 1.2 to 4.7 wt.% for lherzolites (0.18 wt.% for dunite NP-MP05-160B and 11.9 wt.% for websterite NP-MP05-69) (Table S3). Major element compositions are consistent with other mantle-derived xenolith suites in the Canadian Cordillera (Fig. 4; Shi et al., 1998; Peslier et al., 2002; Harder and Russell, 2006; Francis et al., 2010) and other continental spinel-bearing peridotites worldwide, reflecting varying degrees of melt extraction from a fertile mantle source (Peslier et al., 2002).

Trace and rare earth element (REE) compositions (Fig. 5; Table S3) are like other mantle suites from the Canadian Cordillera and show no pronounced single element anomalies. Rare earth element patterns are light rare earth element (LREE; La to Sm) depleted to flat (Fig. 5A–B). Many patterns show a 'spoon-shaped' profile of LREE depletion, with slight enrichment of the lightest REEs (e.g., La, Ce); only one pattern (the harzburgite) is weakly LREE enriched relative to the middle (MREE; Eu to Ho) and heavy (HREE; Er to Lu) rare earth elements. The dunite is especially demonstrative of LREE enrichment; the LREE contents are like that of some other xenoliths from the suite, while the MREE and HREE concentrations are below detection.

Tb/Yb ratios for peridotites (Fig. 5C) can be indicative of whether melt extraction has occurred in the spinel or garnet stability field, as Yb partitions strongly into garnet as a residual phase, resulting in strong Tb/Yb decreases even at small degrees of melting (Bodinier et al., 1988). The Mt. Preston peridotite compositions are consistent with melt extraction in the spinel stability field (Fig. 5C), as with other suites in the Cordillera (Peslier et al., 2002). Terbium enrichment has been interpreted as the result of significant metasomatism (Peslier et al., 2002). None of the Mt. Preston xenoliths analyzed show Tb enrichment over Yb relative to chondrite, suggesting that metasomatic processes did not

disturb the MREEs or if so, very little. We found no correlation between the degree of melt depletion or metasomatism with the mantle equilibration temperatures (section 5 below) as color coded in Figures 5B and 5C.

5.2. Stable isotopes (C–O)

Carbon and oxygen isotope compositions of carbonate from the mantle xenoliths (Table 1), the host basanite (Table S1), and the wall rocks (Table S4) are plotted in Figure 6. Isotopic analyses were performed on leachates of bulk-rock powders and, in the case of dyke and country rock, also on carbonate recovered by micro-drilling of carbonate-rich phases. The wall rock sample was collected <20 m away from the basanite. Carbonate recovered from these three sources (mantle xenoliths, dyke, wall rock) have distinct carbon-oxygen isotopic compositions. Dyke carbonate has $\delta^{18}O_{VSMOW}$ compositions of 13.7 to 14.3 ‰, and $\delta^{13}C_{VPDB}$ compositions of -3.8 to -4.5 ‰. In the dyke, $\delta^{18}O_{VSMOW}$ values are ~17 ‰ greater than wall rock indicating isotopically distinct sources for the carbonate in the dyke and the wall rock (Fig. 6). The isotopic compositions of the carbonates from the dyke are consistent with unaltered magmatic carbonate (e.g., Lee et al., 2000). Additionally, there is no distinction between bulk-rock and micro-drilled analyses of carbonate from the dyke indicting a single (magmatic) isotopic source. The $\delta^{18}O_{VSMOW}$ values for the silicate fraction of the dyke are ~6 ‰ and close to mantle values (i.e. PIC field Fig. 6A).

The wall rock carbonate has $\delta^{18}O_{VSMOW}$ compositions of -1.7 to -2.6 ‰, and $\delta^{13}C_{VPDB}$ compositions of -5.4 to -5.9 ‰. The $\delta^{18}O$ composition of wall rock carbonate (~2 ‰ less than VSMOW) is consistent with equilibration with meteoric water. In contrast, the carbonate within the dyke shows no signs of isotopic exchange with meteoric waters, as isotopic exchange with these fluids would deplete the carbonate in ^{18}O.

Carbonate recovered from fourteen mantle xenoliths plot as two distinct groups based on their ^{13}C compositions (Fig. 6A). The ^{13}C-enriched group has $\delta^{13}C$ compositions between -3.4 and -4.4 ‰ (VPDB), while the ^{13}C-depleted group (7 xenoliths) has $\delta^{13}C$ compositions between -5.7 and -6.1 ‰ (VPDB). Both groups have similar ranges (10.3 to 12.5 ‰ (VSMOW)) of $\delta^{18}O$. All but two of the mantle xenolith samples used for stable isotope analysis contained both granular carbonate and carbonate veins. The other two contained

only vein carbonate and they are part of the ^{13}C-depleted group.

The carbonates from the Mt. Preston mantle xenoliths are closer to primary mantle isotopic compositions than other reported mantle-hosted carbonates (Fig. 6B; Lee et al., 2000; van Achterbergh et al., 2002; Demény et al., 2004; Ducea et al., 2005; Perkins et al., 2006). The Mt. Preston xenoliths contain carbonate having $\delta^{18}O$ compositions less than 3 ‰ greater than the PIC field for primary mantle-derived carbonatites (Fig. 6B; Taylor et al., 1967; Keller and Hoefs, 1995). In other studies, authors report enriched $\delta^{18}O$ compositions in mantle-derived carbonate in xenoliths (Lee et al., 2000; van Achterbergh et al., 2002; Demény et al., 2004; Ducea et al., 2005; Perkins et al., 2006) that are interpreted to indicate isotopic disequilibrium between carbonate and host silicates and explained by short durations between enrichment and eruption. The carbonate in Mt. Preston xenoliths shows less enriched $\delta^{18}O$ compositions (i.e. less isotopic disequilibrium) perhaps indicating longer mantle residence times prior to entrainment by the basanite magma.

5.3. Radiogenic Isotopes (Sr)

Figure 6C shows the $^{87}Sr/^{86}Sr$ ratios of the carbonates in the Mt. Preston xenoliths (Table 1) against their $\delta^{18}O$ composition. The carbonate fraction in the Mt. Preston xenoliths have radiogenic $^{87}Sr/^{86}Sr$ ratios of 0.7044 to 0.7046 and overlap the most enriched xenoliths in the Tasse xenolith suite from the southern Canadian Cordillera (Polat et al., 2018; $^{87}Sr/^{86}Sr$ ~0.7034 to 0.7045). However, both the Tasse suite and the Mt. Preston suite are slightly more radiogenic than other average values for xenoliths suites reported within other southern Canadian Cordillera by Sun et al. (1991) (Jacques Lake: $^{87}Sr/^{86}Sr$ ~ 0.7027, Big Timothy Mountain: $^{87}Sr/^{86}Sr$ ~ 0.7030, West Kettle River: $^{87}Sr/^{86}Sr$ ~ 0.7033, Lassie Lake: $^{87}Sr/^{86}Sr$ ~ 0.7037). The Mt. Preston dyke is slightly less radiogenic (silicate portion: $^{87}Sr/^{86}Sr$ ~0.7036, carbonate portion: $^{87}Sr/^{86}Sr$ ~0.7040; Fig. 6C; Table S1) and has a source composition for carbonate distinct from of the metavolcanic wall rocks ($^{87}Sr/^{86}Sr$ ~0.7047). These $^{87}Sr/^{86}Sr$ values recovered from the Mt. Preston dyke are within the upper range of previously reported Canadian Cordilleran (xenolith-hosting) alkaline basalts ($^{87}Sr/^{86}Sr$ = 0.7024–0.7041; Polat et al., 2018; Sun et al., 1991). The $\delta^{18}O$ composition of the silicate fraction of the Mt. Preston basanite (5.8 to 6.5 ‰ VSMOW; Fig. 6C) is very close to the global mantle average for silicate phases in spinel peridotite xenoliths (5-5.7 ‰ VSMOW).

6. Geothermometry

Mineral chemical compositions of coexisting grains of clinopyroxene (cpx) and orthopyroxene (opx) in 51 xenoliths were measured by electron microprobe (Table S6a), for the purposes of two-pyroxene geothermometry based on the Brey and Köhler (1990) (BK90) calibration. Our approach was to perform thermometry on sequential batches of 5 samples and continue expanding the population until there was no further change in the maximum and minimum temperature (Fig. 7A; see Harder and Russell, 2006). We suggest that the results from 51 samples closely approximate the entire temperature range within the underlying mantle lithosphere.

The Brey and Köhler (1990) geothermometer has a temperature gradient with pressure of ~1.5–1.8 ˚C/Kb. However, we assume that all xenoliths record temperatures along a model geotherm thereby removing the need to adopt an arbitrary pressure for the geothermometric calculations. Operationally we do this by solving the BK90 equation simultaneously with the equation for the model geotherm (see below). The geothermometry results (Table S5) record paleo-temperatures between 815±18 °C and 1119 ±7 °C although most samples record temperatures between ~850 and 950 °C (Fig. 7A). Two xenoliths contain plagioclase and spinel which coexist over a restrictive range of P–T conditions in most mantle assemblages. Geothermometry on these samples returned relatively low equilibrium temperatures of 850°C (NP-MP05-69) and 874°C (NP-MP05-96). The overall distribution of temperatures suggests that the shallower mantle lithosphere is better represented (i.e. more efficiently sampled) than the deep lithosphere. Conversely, the restricted distribution may simply indicate poor mixing of xenolith populations during dyke transport, in contrast to the efficient mixing processes that attend eruption (Russell and Jones, 2023).

The $\delta^{13}C$ isotopic compositions of xenolith-hosted carbonate indicate two groups, relatively enriched ($\delta^{13}C$ ~ -3.4 to -4.4 ‰ (VPDB)) and depleted ($\delta^{13}C$ ~ -5.7 to -6.1 ‰ (VPDB)) (Fig. 6A–B; Table 1). This suggests that the carbonate preserved throughout ~25 km of mantle lithosphere beneath this western margin of the Canadian Cordillera derives from multiple sources (or events). The two groups have similar oxygen isotopic compositions

($\delta^{18}O$ of 10.3 to 12.5 ‰ (VSMOW)) and record overlapping mantle lithosphere temperatures: 851 to 979 °C (+ one at 1119 °C) *vs*. 849 to 940 °C, respectively.

7. Discussion

7.1. Geotherm and Carbonated Mantle Lithosphere

Plotting the xenolith equilibration temperatures on a model steady-state geotherm is a means of mapping the distribution of carbonated mantle within the mantle, estimating the minimum thickness of mantle lithosphere, and constraining the depth to the lithosphere-asthenosphere boundary (LAB). Here, we use a one-dimensional model for the lithosphere comprising a crust of known thickness (Z_M) and having constant thermal conductivity (K_1 = 2.5 W/m·K), and surface heat flow (qo) and surface temperature (To ~10° C). The crustal layer has an exponential distribution of radiogenic heat producing elements ($A(z) = A_O\, e^{-z/Z_M}$; Russell and Kopylova, 1999) and we consider a range of heat production (Ao) values. The underlying mantle lithosphere has constant thermal conductivity (K_2 = 3.2 W/m·K) and no radiogenic heat source. The lithospheric crust and mantle are coupled numerically by a common Moho temperature (T_M) and the reduced heat flow (q_M) at the Moho.

The temperature distribution as a function of depth (z) in the crust is described by:

$$T(z) = T_0 + \frac{q_0\, z}{K_1} + \frac{Ao\, Z_M^2}{K_1}\left(1 - \frac{z}{Z_M} - e^{-z/Z_M}\right) \qquad 0 < z < Z_M \ . \quad (1)$$

Values of q_0 are coupled to the form of the heat production equation and dictated by the relationship (Russell and Kopylova, 1999):

$$q_0 = 0.3679\, Z_M\, Ao + \frac{(T_M - T_0)\, K_1}{Z_M} \qquad (2)$$

and, therefore, also dependent on the depth and temperature of the Moho. The expected steady-state temperature distribution in the mantle lithosphere is described by:

$$T(z) = T_M + \frac{[q_0 - 0.6321\, Ao\, Z_M]}{K_2}\,(z - Z_M) \qquad Z_M < z < Z_a \ . \qquad (3)$$

We have assumed a Moho depth (Z_M) of 32 km (Calkins et al., 2010) and an average crustal heat production of 1.6 ±0.8 μW/m^3 (Lewis et al., 2003) which also fixes values of q_0 (Eq. 2).

Model values of q_0 for the range of Ao values (0.8 to 2.4 μW/m^3) vary from 63 to 90 mW/m^2 which agrees well with average measured values reported for the Canadian Cordillera (76 ±21 mW/m^2; e.g., Hyndman, 2017).

We assume Moho temperature (T_M) to be equal to, or lower than, the lowest temperature xenolith (815°C) and have adopted a value of 800°C (Fig. 7). Similarly, the highest temperature xenolith (1119°C) constrains the minimum temperature of the LAB (Fig. 7B). A model geotherm is shown in Figure 7B for three separate values of Ao. The model values of q_0 are inversely correlated to values of Ao such that the highest temperature xenolith corresponds to depths of 49 km (low Ao and high q_0) or 58 km (high Ao and low q_0) implying minimum thicknesses of the mantle lithosphere of 17-26 km. The reduced heat flow at the base of the crust (q_M) would be 61 to 41 mW/m^2 for low to high values of Ao (i.e. inverse correlation). These values of q_M correspond to temperature gradients in the mantle of 19 to 13 °C km^{-1}, respectively.

An alternative estimate of lithosphere thickness can be made by extrapolating the model geotherms to intersect the adiabat based on values adopted by Hyndman and Canil, 2021 (after Katsura et al., 2010). The three model geotherms (Fig. 7B) intersect the adiabat at depths of 58 (low Ao) to 72 (hi Ao) km implying mantle lithosphere thicknesses of between 26 and 40 km and LAB depths between 58–72 km and temperatures of 1310–1320 °C. These results accord well with estimates (65 km and ~1350 ºC) from Hyndman and Canil (2021) and Canil and Hyndman (2023).

The model geotherm shows that carbonate is distributed pervasively throughout the entire mantle lithosphere and that the carbonate is a stable mantle phase over a minimum range of temperatures of 800 to 1120 °C and pressures of 0.9 to 1.7 GPa. The carbonate occurs in several habits, but those habits are insensitive to source temperatures, pressures, and depths. Four samples with granular carbonate have temperatures of 850 to 895 °C, ten xenoliths with carbonate veins have temperatures of 826 to 924 °C, and 37 xenoliths contain both habits and have temperatures of 815 to 1119 °C.

7.2. Significance of mantle carbonate

Primary mantle-derived carbonate is rarely preserved in mantle xenoliths but provides important insights on mantle metasomatism involving carbonatitic melts/fluids. At Mt.

Preston, primary carbonate (Mg-calcite; Table S6b) is pervasive and occurs in both lherzolites, websterites, and dunites and the xenoliths preserve strong textural evidence of its mantle equilibration. For example, the intergranular carbonate within the Mt. Preston suite preserves triple-point grain boundaries consistent with textural equilibrium between carbonate and mantle silicates. Other occurrences of carbonate within mantle-derived xenoliths are reported for localities in Argentina (Laurora et al., 2001; Scambelluri et al., 2009), Hungary (Demény et al., 2004; 2010), the Kerguelen Islands (Moine et al., 2004), Spitsbergen (Ionov et al., 1996), the Siberian Craton (Ionov et al., 2018), the East African Rift, Tanzania (Lee et al., 2000), South Africa (Berg, 1986), and the southwest United States (Ducea et al., 2005; Perkins et al., 2006). Most of these occurrences are described as interstitial patches associated with second generation crystallization, or as inclusions within crystals, typically in textural (glass) or isotopic disequilibrium with the host rocks.

In addition, mantle carbonate at Mt. Preston is closely associated with sulphides and, together, are found as intergranular patches, in veins, and as inclusion trails within healed mantle silicates (Fig. 3A–C). Sulphides are a common accessory phase in mantle-derived rocks and are a common component of carbonate melts or carbonate-silicate melts (Ionov et al., 1996). The sulphides found in Mt. Preston mantle xenoliths occur across the full range of equilibration temperatures (i.e. depth) and are found associated with both high and low $\delta^{13}C$ groups of carbonate. This occurrence suggests that carbonate and sulphide result from the same enrichment event(s).

Chemical compositional features of the Mt. Preston xenoliths are also consistent with a carbonate metasomatic agent. Most of the xenoliths show calcium enrichment relative to aluminum, which has been attributed to cryptic carbonate metasomatism (Peslier et al., 2002). Many REE patterns from the Mt. Preston xenoliths show slight enrichment of the lightest REEs, consistent with the effects of a migrating LREE-rich melt such as carbonatite. Collectively, the petrographic observations and geochemical data strongly support the premise that carbonate and sulphide accessory phases are part of the pre-entrainment mantle paragenesis.

Measured $\delta^{18}O$ vs. $\delta^{13}C$ compositions for the Mt. Preston xenolith and dyke carbonates are close to bulk mantle compositions and distinct from the wall rock carbonates

(Fig. 6B). In fact, the $\delta^{13}C$ and $\delta^{18}O$ isotopic compositions of Mt. Preston carbonate are closer to primary mantle compositions than many other occurrences of mantle-hosted carbonates (Fig. 6B; Lee et al., 2000; van Achterbergh et al., 2002; Demény et al., 2004; Ducea et al., 2005; Perkins et al., 2006). Oxygen isotopic compositions can be more easily re-equilibrated, yet the measured $\delta^{18}O$ values for xenolith, dyke, wall rock plot as discrete clusters (Fig. 6A) and show no indication of chemical mixing between sources; there is also no evidence for meteoric alteration of the xenoliths nor dyke.

$\delta^{13}C$ values for the Mt. Preston peridotite xenoliths are like carbonate-bearing mantle xenoliths from New Mexico (Lee et al., 2000) and other localities (Fig. 6B) but have even more mantle-like $\delta^{18}O$ compositions. This may suggest relatively better preservation of primary carbonate within the Mt. Preston suite. Furthermore, the Mt. Preston mantle-carbonate samples define two distinct groups suggesting at least two carbonate-sulphide melt enrichment events. The concept of multiple enrichment events is further supported by slight differences in the $^{87}Sr/^{86}Sr$ isotopic compositions of the two $\delta^{13}C$-defined populations (high-C 0.7044 *vs*. low-C 0.7046). In addition, differences in $^{87}Sr/^{86}Sr$ for the carbonate and silicate fractions of the dyke could indicate mixing of $^{87}Sr/^{86}Sr$ compositions between dyke silicates and xenolith carbonate, thereby preserving evidence for a magma charged with CO_2 derived, in part, from mantle-derived (i.e. xenolith) carbonate (see below).

7.3. Source of Carbonatite Metasomatism

Studies of the mantle lithosphere underlying the Canadian Cordillera have shown it to be relatively uniform in composition, thermal regime, and age (e.g., Francis et al., 2010 and references therein). Rhenium-osmium dating of lithospheric mantle-derived xenoliths (Peslier et al., 2000) has recovered Proterozoic model ages across the Canadian Cordillera, consistent with melt depletion events occurring within a short timeframe for the Cordilleran lithospheric mantle. Whether autochthonous or allochthonous this indicates a common melting history for, at least, the lithospheric mantle underlying the southeast Canadian Cordillera. This result precludes the suggestion of a simple extension of cratonic crust coupled to its own lithospheric mantle residing beneath the eastern Cordillera, as the mantle lithosphere in that region appears to be much younger than the wedge of cratonic crustal basement that overlies it (Peslier et al., 2000).

The Mt. Preston xenolith suite is in a unique geographic location on the western margin of the Intermontane Belt compared to other BC cordilleran xenolith localities which are further from the continental margin. They are also the only mantle peridotite xenoliths in the BC cordillera that preserve primary, mantle-equilibrated carbonates (and associated sulphides). Furthermore, these carbonated mantle xenoliths are the only ones reported from the Pacific Coast Ranges of the western margin of North America. The carbonates and sulphides are texturally undisturbed suggesting that the metasomatic event was the last event prior to entrainment by the 19 Ma basanite magma. This suggests a different history involving a geographically restricted enrichment process that probably involved metasomatic agents related to subduction of oceanic crust along the central western margin of BC.

One possible source of carbonatitic metasomatism of the mantle lithosphere is subduction of carbonate in sediments coupled to the down going slab. Subducting slab-related enrichment agents have been interpreted for other carbonate bearing xenolith suites (e.g. Laurora et al., 2001; Demény et al., 2004; Ducea et al., 2005; Perkins et al., 2006). Decarbonation reactions in subducting plates can occur at higher temperatures than dehydration reactions, based on experimental and thermodynamic data (Yaxley and Green, 1994; Ducea et al., 2005 and references therein), or the silicate and carbonate melts may be immiscible resulting in separation. Subduction-related metasomatism has been considered for xenolith suites from northwest BC and southwest Yukon based on incompatible trace element enrichments, although no metasomatic phases were observed in those rocks (Shi et al., 1998; Peslier et al., 2000). If subduction-related enrichment during Coast Plutonic Complex magmatism is the source for the carbonates and sulphides in the Mt. Preston suite, the sites in northwest BC and southwest Yukon might be expected to show this as well. However, several of these sites are interpreted to overlie anomalously hot asthenosphere interpreted as a Tertiary to recent thermal event (Frederiksen et al., 1998; Shi et al., 1998); at the interpreted P–T range for these rocks little isobaric heating (≤50 °C) is required to make crystalline calcite unstable.

Mt. Preston occupied an arc to back-arc location during the duration of Coast Plutonic Complex magmatism history. Based on tectonic models (van der Heyden, 1992; Monger et al., 1994; Gehrels et al., 2009), this would restrict the timing of the enrichment event(s) from

528 at earliest, Jurassic time to ~50 Ma when Coast Belt magmatism waned; subduction ended
529 ~40 Ma, although the margin of the subducted slab persisted to ~35 Ma beneath the area
530 (Madsen et al., 2006). However, for metasomatic enrichment to have occurred before 90–85
531 Ma the mantle lithosphere under Mt. Preston would have had to be thermally and texturally
532 unaffected by the accretion of terranes of the Insular Belt into Stikinia–Yukon Tanana (e.g.,
533 Monger et al., 1982; Gehrels et al., 2009).

534 The $^{87}Sr/^{86}Sr$ values for Mt. Preston samples are slightly more radiogenic than
535 expressed by the eastern BC xenolith suites. The more radiogenic $^{87}Sr/^{86}Sr$ ratios might be
536 indicative of carbonatite metasomatism or the lower $^{87}Sr/^{86}Sr$ ratios for the eastern BC
537 xenoliths could reflect the region's proximity to the North American Craton margin. Isotopic
538 evidence suggests that the Cordilleran lithosphere may not be as uniform as previously shown
539 (Peslier et al., 2000; Francis et al., 2010). In particular, the Mt. Preston carbonated peridotite
540 samples imply important compositional variations within the Canadian Cordilleran mantle
541 lithosphere that inform on the mantle's volatile budget (carbon), the fate of subducted carbon,
542 and its release during volcanism (discussed in section 7.4). The stability of carbonate, in the
543 mantle, for example, has been shown to be redox controlled (e.g., Frost & McCammon, 2008),
544 suggesting variations in the oxidation state of mantle material beneath the Intermontane–
545 Coast Belt margin in the western Cordillera.
546

547 7.4. Carbonate Preservation and Ascent

548 Carbonated peridotitic mantle is the common source for a wide variety of mantle-
549 derived magmas including carbonatites, nephelinites, basanites, melilitites, and kimberlites
550 (e.g., Dasgupta et al. 2013). Given Earth's abundance of these Si-undersaturated, CO_2-rich
551 magmas it is surprising that carbonate-bearing samples of mantle lithosphere are relatively
552 rare. This discrepancy led Canil (1990) to perform a series of decompression experiments
553 designed to explore the carbonate stability during ascent and to assert that carbonate
554 decomposes during decompression at rates (1.5–3 GPa h^{-1}) exceeding feasible magma ascent
555 velocities (12–25 m s^{-1}).

556 This raises the question of how the carbonate in these xenoliths was preserved during
557 ascent of the Mt. Preston basanite magma. All samples of the mantle beneath Mt. Preston

were carbonated and equilibrated at pressures less than 2 GPa and at temperatures lower than the basanite magma (<1250ºC). In this environment, carbonate can be destroyed in at least three ways: i) by solid state reaction to produce a non-carbonate assemblage, ii) by decomposition to a fluid or gas driven by changes in pressure, temperature, or P_{CO2} (Canil 1990; Escardino et al., 2013; Frost & McCammon, 2008), or iii) by dissolution or assimilation in a silicate melt (Edwards and Russell, 1998). To preserve the carbonate and sulphides in the xenoliths, xenolith transport rates must have exceeded rates of thermal-chemical processes promoting carbonate destruction (i.e. decomposition, melt infiltration, etc.).

There is every evidence that the basanite magma transited the mantle lithosphere rapidly. The basanite is essentially aphyric indicating that near liquidus temperatures (~1250ºC) were maintained throughout transport, implying little loss of enthalpy; ascent rates exceeded rates of conductive cooling to the wall rocks. The basanite magma (ρ_x ~2700 kg m^{-3}) also transported dense (ρ_x ~3300 kg m^{-3}; Table S5) mantle xenoliths sourced from depths of 70–30 km to within several kilometers of the Earth's surface. Several of the largest xenoliths are ~50 cm in diameter. The abundance and size range of xenoliths carried by a low viscosity melt (η ~25 Pa s) within a relatively narrow dyke (1–3 m) also support a relatively high ascent rate (e.g., Sparks et al., 2004). For our example calculations below we adopt a physically reasonable value of ~4 m s^{-1} (see Sparks et al., 2004; Russell and Jones, 2023).

There are two main arguments for the preservation of the carbonate in this suite of mantle xenoliths. The first concerns the thermal history of the xenoliths from the depth of sampling to the shallow crust (cf. Mitchell et al., 1980). Decomposition of carbonate is strongly dependent on temperature; as xenoliths are heated above their ambient mantle temperatures by the host basanite, rates of carbonate decomposition will increase (L'vov, 2007; Escardino et al., 2013). We have modelled the heating times (t_h) of the mantle xenoliths and compared those times to their residence times (t_r) at a prescribed ascent rate (V_m ~4 m s^{-1}; Fig. 8A). Xenolith residence times are dictated by magma rise rate, their settling rates (i.e. size of xenolith), and their source depth (Fig. 8B; Russell and Jones, 2023). Values of t_r are

greatest for large xenoliths sourced from greatest depths (Fig. 8A) whilst V_m sets limits on the maximum size of xenolith that can be carried. Xenolith rise rates (V_x) are computed as:

$$V_x = V_m + V_s \qquad (4)$$

where V_s represents the sinking rate of the xenolith relative to the melt which, for the purposes of demonstration, is approximated here by Stokes terminal settling velocity. Heating times are the times required to heat spherical xenoliths of different sizes to a core temperature > 1250°C assuming conductive heating (e.g., Carslaw and Jaeger, 1959; pg. 233; Mitchell et al., 1980) and an initial temperature based on their position along the geotherm (i.e. depth-temperature; Fig. 8B).

There is a window in terms of xenolith size and source depth where carbonate is preserved (Fig. 8D). Carbonate preservation is favoured when $t_h > t_r$. Smaller xenoliths (i.e. D < 10 cm) typically have $t_h < t_r$ regardless of sample depth because heating times are short (Fig. 8C). In contrast, 50 cm diameter xenoliths have substantial heating times relative to their rise rates ($t_r < t_h$) except when sourced near the LAB (Fig. 8C). There transit times are greatest, and the ambient temperature is highest thereby reducing t_h values. However, slightly larger xenoliths (D ~ 55 cm) are settling more rapidly and have high values of t_r, such that $t_r >> t_h$ regardless of sample depth. For minimum magma ascent rates of 4 m s^{-1}, xenoliths that are between 20 and 45 cm in size (diameter) are optimal for preserving carbonate (Fig. 8D).

The second way in which carbonate decomposition is mitigated relates to the intrinsic volatile content of the host magma. Carbonate decomposition rates are strongly dependent on the composition of ambient atmosphere; high values of P_{CO2} cause a hyperbolic decrease in carbonate decomposition rate (L'vov, 2007). Experimental data of Escardino et al. (2013) showed calcite decomposition in a CO_2 atmosphere to practically stop at temperatures < 875 °C; at higher temperatures decomposition rates dropped by > 80%. The basanite dyke contains magmatic groundmass carbonate and is vesicular indicating it was CO_2-volatile rich. Despite the low solubility of CO_2 at crustal pressures, the magma trapped in the dyke was not fully degassed but, rather, remained enriched in CO_2. The ascent rates were sufficiently high to effectively suppress efficient degassing of CO_2 implying a high partial pressure of CO_2 throughout transport that would inhibit carbonate decomposition.

Lastly, all samples of mantle lithosphere from beneath Mt. Preston are carbonated regardless of depth. Olivine and pyroxene xenocrysts in the basanite result from xenolith disaggregation during transport which potentially allowed for scavenging and chemical assimilation of xenolith-hosted carbonate (e.g., Ionov et al., 1996; Lee et al., 2000; Laurora et al., 2001). Disaggregation of carbonated peridotite xenoliths during transport represents an efficient mechanism for liberation of accessory carbonate leading to increased CO_2 solubility or suppression of degassing of the rising magma. The additional dissolved or exsolved CO_2 content would increase magma buoyancy, support higher ascent rates for both the magma and its entrained xenoliths, thereby enhancing carbonate preservation. The carbon, oxygen, and strontium isotopic compositions of the dyke and xenolith carbonate are consistent with this process. For example, the carbonate sampled from the basanite dyke has a $\delta^{13}C$ composition within the range of the sampled mantle xenoliths, and has a $^{87}Sr/^{86}Sr$ composition between the dyke silicate minerals and the xenolith carbonate.

8. Summary

The 19 My basanite dyke exposed near Mt. Preston, British Columbia intrudes metavolcanic rocks (Hazelton Group) of the western Intermontane Belt and is situated within 40 km of Coast Belt. The dyke contains abundant spinel-bearing peridotite (mainly lherzolite) xenoliths from the underlying Cordilleran mantle. The xenolith suite is unique for preserving primary, mantle-equilibrated magnesian calcite as an accessory phase commonly in association with sulphides (pentlandite and chalcopyrite). Two-pyroxene thermometry (N=51) returned a range of paleo-temperature estimates limiting the Moho temperature to $\leq$ 815 ºC and the LAB temperature to $\geq$ 1120 ºC. A model geotherm, coupled with the geothermometry and projected to the mantle adiabat, constrains the mantle lithosphere to a thickness of 26 to 40 km, and the LAB to a depth of 58 to 72 km and temperature of 1310–1320 ºC (see also Hyndman and Canil, 2021). The thermometry also shows that accessory carbonate and sulphide phases are stable throughout mantle lithosphere at temperatures of ~800 –1120ºC corresponding to pressures (i.e. depths) of ~1–1.7 GPa. The carbonate-sulphide assemblage provides strong evidence for pervasive metasomatism of an earlier melt-depleted mantle lithosphere involving at least two

isotopically distinct carbonatitic fluids with associated monosulphides (rather than hydrous silicate fluids). The metasomatic event derived from subduction of oceanic crust beneath the western margin of the Canadian Cordillera during Coast Plutonic Belt magmatism, when Mt. Preston was in an arc to back arc position (between ~90 and 35 Ma). Rapid magma transport rates combined with a high intrinsic P_{CO2}, sustained by scavenging of carbonated mantle lithosphere, provided the means to preserve the accessory carbonate within these entrained fragments of mantle lithosphere.

Acknowledgements

We thank the guest editors Kelin Wang, Claire Currie, and John Cassidy for the opportunity to contribute to the special issue of the Canadian Journal of Earth Sciences in honour of Roy Hyndman: "Geophysical studies of the lithosphere and plate boundaries". Our manuscript benefitted from critical reviews by Cliff Shaw and an anonymous referee and editorial guidance from Claire Currie.

Competing interests

The authors declare that they have no known competing financial interests or personal relationships that may have influenced the work reported in this paper.

Data availability

All data is available in the supplementary material associated with the manuscript or from the authors.

Funding

This research was funded by the Natural Sciences and Engineering Research Council (NSERC) Discovery Grant held by JKR and the NSERC Collaborative Research Opportunities (CRO) grant (BATHOLITHS). NP acknowledges research grants awarded by the Geological Society of America and the Mineralogical Association of Canada.

References

Asimow, P.D., Ghiorso, M.S., 1998. Algorithmic modifications extending MELTS to calculate subsolidus phase relations. Am. Min. 83, 1127-1131. doi:10.2138/am-1998-9-1022

Barker, D.S., 1996. Consequences of recycled carbon in carbonatites. Can. Min. 34, 373-387.

Brey, G. P., Köhler, T., 1990. Geothermobarometry in four-phase lherzolites II. New thermobarometers, and practical assessment of existing thermobarometers. J. Petrol. 31, 6, 1353-1378. doi:10.1093/petrology/31.6.1353

Calkins, J. A., Zandt, G., Girardi, J., Dueker, K., Gehrels, G. E., Ducea, M. N., 2010. Characterization of the crust of the Coast Mountains Batholith, British Columbia, from P to S converted seismic waves and petrologic modeling. Earth Planet. Sci. Lett. 289, 145-155. doi:10.1016/j.epsl.2009.10.037

Canil, D., 1990. Experimental study bearing on the absence of carbonate in mantle-derived xenoliths. Geology 18, 1011-1013.

Canil, D., Scarfe, C.M., 1989. Origin of phlogopite in mantle xenoliths from Kostal Lake, Wells Gray Park, British Columbia. J. Petrol. 30, 1159-1179. doi:10.1093/petrology/30.5.1159

Canil, D., Hyndman, R.D., 2023. Equilibration depth and temperature of Neogene alkaline lavas in the Cordillera of Alaska and Canada as a constraint on the lithosphere–asthenosphere boundary. Can. J. Earth Sci. 60, 1206-1222. doi:10.1139/cjes-2023-0005

Carslaw, H.S., Jaeger, J.C., 1959. Conduction of Heat in Solids. Clarendon Press, Oxford.

Clinton, R.N., Mayeda, T.K., 1963. The use of bromine pentafluoride in the extraction of oxygen from oxides and silicates for isotopic analysis. Geochimica et Cosmochimica Acta 27, 43-52. doi:10.1016/0016-7037(63)90071-1

Dasgupta, R., Mallik, A., Tsuno, K., et al. 2013. Carbon-dioxide-rich silicate melt in the Earth's upper mantle. Nature 493, 211–215. doi:10.1038/nature11731

Deines, P., 2002. The carbon isotope geochemistry of mantle xenoliths. Earth-Science Reviews 58, 247-278. doi:10.1016/S0012-8252(02)00064-8

Delpech, G., Lorand, J. P., Grégoire, M., Cottin, J. Y., O'Reilly, S. Y., 2012. In-situ geochemistry of sulfides in highly metasomatized mantle xenoliths from Kerguelen, southern Indian Ocean. Lithos 154, 296-314. doi:10.1016/j.lithos.2012.07.018

Demény, A., Vennemann, T. W., Hegner, E., Nagy, G., Milton, J. A., Embey-Isztin, A., Homonnay, Z., Dobosi, G., 2004. Trace element and C–O–Sr–Nd isotope evidence for subduction-related carbonate–silicate melts in mantle xenoliths (Pannonian Basin, Hungary). Lithos 75, 89-113. doi:10.1016/j.lithos.2003.12.016

Demény, A., Dallai, L., Frezzotti, M.-L., Vennemann, T.W., Embey-Isztin, A., Dobosi, G., Nagy, G., 2010. Origin of CO_2 and carbonate veins in mantle-derived xenoliths in the Pannonian Basin. Lithos 117, 172-182. doi:10.1016/j.lithos.2010.02.013

Diakow, L.J., Mahoney, J.B., Haggart J. W., and 6 others, 2003. Geology of the Eastern Bella Coola Map Area (93 D), West-Central British Columbia. In Geological Fieldwork 2002, BC Ministry of Energy and Mines, Paper 2003-1, 65-76.

Ducea, M. N., Saleeby, J., Morrison, J., Valencia, V. A., 2005. Subducted carbonates, metasomatism of mantle wedges, and possible connections to diamond formation: An example from California. Am. Mineral. 90, 864-870. doi:10.2138/am.2005.1670

Edwards, B., Russell, J. K., 1998. Time scales of magmatic processes: new insights from dynamic models for magmatic assimilation. Geology 26, 1103–1106.

Edwards, B., Russell, J. K., 2000. Distribution, nature, and origin of Neogene-Quaternary magmatism in the northern Cordilleran volcanic province, Canada. Geol. Soc. Am. Bull. 112, 1280–1295.

726 Escardino, A., García-Ten, J., Feliu, C., Saburit, A., Cantavella, V., 2013. Kinetic study of
727 the thermal decomposition process of calcite particles in air and CO_2 atmosphere. J.
728 Ind. Eng. Chem. 19, 886-897. doi:10.1016/j.jiec.2012.11.004
729 Francis, D., Ludden, J., 1995. The signature of amphibole in mafic alkaline lavas, a study in
730 the Northern Canadian Cordillera. J. Petrol. 36, 1171-1191.
731 doi:10.1093/petrology/36.5.1171
732 Francis, D., Minarik W., Proenza Y., Shi, L., 2010. An overview of the Canadian
733 Cordilleran lithospheric mantle. Can. J. Earth Sci. 47, 353-368. doi:10.1139/E09-
734 072
735 Frederiksen, A. W., Bostock, M. G., VanDecar, J. C., Cassidy, J. F., 1998. Seismic
736 structure of the upper mantle beneath the northern Canadian Cordillera from
737 teleseismic travel-time inversion. Tectonophys. 294, 43-55. doi:10.1016/S0040-
738 1951(98)00095-X
739 Frost, D. J., McCammon, C. A., 2008. The redox state of Earth's mantle. Annu. Rev. Earth
740 Planet. Sci., 36, 389-420. doi:10.1146/annurev.earth.36.031207.124322
741 Gehrels, G., Rusmore, M., Woodsworth, G., Crawford, M., Andronicos, C., Hollister, L.,
742 Patchett, J., Ducea, M., Butler, R., Klepeis, K., Davidson, C., Friedman, R.,
743 Haggart, J., Mahoney, B., Crawford, W., Pearson, D., Girardi, J., 2009. U-Th-Pb
744 geochronology of the Coast Mountains batholith in north-coastal British Columbia:
745 constraints on age and tectonic evolution. Geol. Soc. Am. Bull. 121, 1341-1361.
746 doi:10.1130/B26404.1
747 Ghent, E.D., Edwards, B.R., Russell, J.K., 2019. Pargasite-bearing vein in spinel lherzolite
748 from the mantle lithosphere of the North America Cordillera. Can. J. Earth Sci. 56,
749 870-885. doi:10.1139/cjes-2018-0239
750 Gordee S. M., Mortensen J. K., Mahoney J. B., Hooper R. L. 2005. Volcanostratigraphy,
751 lithogeochemistry and U-Pb geochronology of the upper Hazelton Group, west-
752 central British Columbia: implications for Eskay Creek – type VMS mineralization
753 in southwest Stikinia. In Geological Fieldwork, 2004, British Columbia Ministry of
754 Energy, Mines and Petroleum Resources, Paper 2005-1, pp. 311–322.
755 Harder, M., Russell, J. K., 2006. Thermal state of the upper mantle beneath the Northern
756 Cordilleran Volcanic Province (NCVP), British Columbia, Canada. Lithos 87, 1-
757 22. doi:10.1016/j.lithos.2005.05.002
758 Harmon, R. S., Hoefs, J., 1995. Oxygen isotope heterogeneity of the mantle deduced from
759 global ^{18}O systematics of basalts from different geotectonic settings. Contrib.
760 Mineral. Petrol. 120, 95-114. 126 doi:10.1007/BF00311010
761 Hunter, E.A., Hunter, J.R., Zajacz, Z., and 4 others, 2020. Vapor transport and deposition
762 of Cu-Sn-Co-Ag alloys in vesicles in mafic volcanic rocks. Econ. Geol. 115, 279-
763 301. doi:10.5382/ECONGEO.4702
764 Hyndman, R.D., 2017. Lower-crustal flow and detachment in the North American
765 Cordillera: a consequence of Cordillera-wide high temperatures. Geophys. J. Int.
766 209, 1779–1799, https://doi.org/10.1093/gji/ggx138
767 Hyndman, R.D., Canil, D., 2021. Geophysical and geochemical constraints on Neogene-
768 Recent volcanism in the North American Cordillera Geochem. Geophys. Geosys.
769 22, e2021GC009637. https://doi.org/10.1029/2021GC009637
770 Ionov, D. A., O'Reilly, S. Y., Genshaft, Y. S., Kopylova, M. G., 1996. Carbonate-bearing

771 mantle peridotite xenoliths from Spitsbergen: phase relationships, mineral
772 compositions and trace-element residence. Contrib. Mineral. Petrol. 125, 375-392.
773 doi:10.1007/s004100050229
774 Ionov, D.A., Shirey, S.B., Weis, D., Brugmann, G., 2006. Os–Hf–Sr–Nd isotope and PGE
775 systematics of spinel peridotite xenoliths from Tok, SE Siberian craton: Effects of
776 pervasive metasomatism in shallow refractory mantle. Earth Planet. Sci. Lett. 241,
777 47-64. doi:10.1016/j.epsl.2005.10.038
778 Ionov, D.A., Doucet, L.S., Xu, Y., Golovin, A.V., Oleinikov, O.B., 2018. Reworking of
779 Archean mantle in the NE Siberian craton by carbonatite and silicate melt
780 metasomatism: Evidence from a carbonate-bearing, dunite-to-websterite xenolith
781 suite from the Obnazhennaya kimberlite. Geochim. Cosmochim. 224, 132-153.
782 doi:10.1016/j.gca.2017.12.028
783 Katsura, T., Yoneda, A., Yamazaki, D., Yoshino, T., Ito, E., 2010. Adiabatic temperature
784 profile in the mantle: Phys. Earth Planet. Inter. 183, 212–218.
785 doi:10.1016/j.pepi.2010.07.001
786 Keller, J., Hoefs, J., 1995. Stable isotope characteristics of recent natrocarbonatites from
787 Oldoinyo Lengai. In: Carbonatite volcanism: Oldoinyo Lengai and the petrogenesis
788 of natrocarbonatites. (eds. K. Bell and J. Keller). Springer, Berlin. pp. 113-123.
789 doi:10.1007/978-3-642-79182-6_9
790 Laurora, A., Mazzucchelli, M., Rivalenti, G., Vannucci, R., Zanetti, A., Barbieri, M. A.,
791 Cingolani, C. A., 2001. Metasomatism and melting in carbonated peridotite
792 xenoliths from the mantle wedge: The Gobernador Gregores Case (Sothern
793 Patagonia). J. Petrol. 42, 1, 69-87. doi:10.1093/petrology/42.1.69
794 Lee, C., Rudnick, R. L., McDonough, W. F., Horn I., 2000. Petrologic and geochemical
795 investigation of carbonates in peridotite xenoliths from northeastern Tanzania.
796 Contrib. Mineral. Petrol. 139, 470-484. doi:10.1007/s004100000144
797 Lewis, T. J., Hyndman, R. D., Fluck, P., 2003. Heat flow, heat generation, and crustal
798 temperatures in the northern Canadian Cordillera: Thermal control of tectonics. J.
799 Geophys. Res. 108, B6, 16-1 – 16-18. doi:10.1029/2002JB002090
800 L'vov, B.V., 2007. Thermal Decomposition of Solids and Melts: New Thermochemical
801 Approach to the Mechanism, Kinetics and Methodology. Dordrecht: Springer
802 Netherlands, http://dx.doi.org/10.1007/978-1-4020-5672-7. doi:10.1007/978-1-
803 4020-5672-7
804 Madsen, J. K., Thorkelson, D. J., Friedman, R. M., Marshall, D. D., 2006. Cenozoic to
805 Recent plate configurations in the Pacific Basin: Ridge subduction and slab window
806 magmatism in western North America. Geosphere 2, 1, 11-34.
807 doi:10.1130/GES00020.1
808 Mahoney J. B., Hooper R. L., Gordee S. M., Haggart J. W., Mortensen J. K. 2005. Initial
809 evaluation of bedrock geology and economic mineralization potential of southern
810 Whitesail Lake map area (NTS 093E/02, 03), west-central British Columbia. In
811 Geological Fieldwork, 2004, British Columbia Ministry of Energy, Mines and
812 Petroleum Resources, Paper 2005-1, pp. 291–299.
813 McDonough, W. F., Sun, S., 1995. The composition of the Earth. Chem. Geol. 120, 223-
814 253. doi:10.1016/0009-2541(94)00140-4
815 Mitchell, R.H., Carswell, D.A., Clarke, D.B., 1980. Geological implications and validity of

816 calculated equilibration conditions for ultramafic xenoliths from the Pipe 200
817 kimberlite, northern Lesotho. Contrib. to Mineral. Petrol. 72, 205–217.
818 doi:10.1007/BF00399481
819 Moine, B. N., Gregoire, M., O'Reilly, S. Y., Delpech, G., Sheppard, S. M. F., Lorand, J. P.,
820 Renac, C., Giret, A., Cottin, J. Y., 2004. Carbonatite melt in oceanic upper mantle
821 beneath the Kerguelen Archipelago. Lithos 75, 239-252.
822 doi:10.1016/j.lithos.2003.12.019
823 Monger, J., Price, R. A., Tempelman-Kluit, D. J., 1982. Tectonic accretion and the origin of
824 the two major metamorphic and plutonic welts in the Canadian Cordillera. Geology
825 10, 70–75.
826 Monger, J., van der Heyden, P., Journeay, J. M., Evenchick, C. A., Mahoney, J. B., 1994.
827 Jurassic-Cretaceous basins along the Canadian Coast Belt: Their bearing on pre-
828 mid- Cretaceous sinistral displacements. Geology 22, 175-178.
829 Naughton, J.J., 1975. Fiber-containing and crystal-lined basaltic vesicles: Possible lunar
830 analogs. Am. Min. 60, 1118–1121.
831 Pearson, D. G., Canil, D., Shirey, S.B. and Carlson. R. W. 2003. Mantle samples included
832 in volcanic rocks: Xenoliths and diamonds, in (Eds. H. D. Holland, K. K. Turekian)
833 Treatise on Geochemistry. Pergammon, 171-275. doi:10.1016/B0-08-043751-
834 6/02005-3
835 Perkins, G. B., Sharp, Z. D., Selverstone, J., 2006. Oxygen isotope evidence for subduction
836 and rift-related mantle metasomatism beneath the Colorado Plateau-Rio Grande rift
837 transition. Contrib. Mineral. Petrol. 151, 633-650. doi:10.1007/s00410-006-0075-6
838 Peslier, A. H., Reisberg, L., Ludden, J., Francis, D., 2000. Os isotopic systematics in
839 mantle xenoliths; age constraints on the Canadian Cordillera lithosphere. Chem.
840 Geol. 166, 85-101. doi:10.1016/S0009-2541(99)00187-4
841 Peslier, A. H., Francis, D., Ludden, J., 2002. The lithospheric mantle beneath continental
842 margins: Melting and melt-rock reaction in Canadian Cordillera xenoliths. J. Petrol.
843 43, 11, 2013-2047. doi:10.1093/petrology/43.11.2013
844 Peterson, N.D., Russell, J.K., Mahoney, J.B. 2006. Mantle-Derived Peridotite Xenoliths
845 from the Western Intermontane Belt, Whitesail Lake map area (NTS 093E),
846 Western BC. Geological Fieldwork, Ministry of Energy, Mines and Petroleum
847 Resources Paper 2006-1, 153-161.
848 Peterson, N.D., 2010. Carbonated mantle lithosphere in the western Canadian Cordillera.
849 University of British Columbia. doi.org/10.14288/1.0052818
850 Polat, A., Frei, R., Longstaffe, F.J., Thorkelson, D.J., Friedman, E., 2018. Petrology and
851 geochemistry of the Tasse mantle xenoliths of the Canadian Cordillera: A record of
852 Archean to Quaternary mantle growth, metasomatism, removal, and melting,
853 Tectonophys. 737, 1-26. doi:10.1016/j.tecto.2018.04.014
854 Pouchou J. L., Pichoir F., 1985. PAP $\phi(\rho Z)$ procedure for improved quantitative
855 microanalysis. Microbeam Analysis 1985, 104-106.
856 Rielli, A., Tomkins, A.G., Nebel, O., Brugger, J., Etschmann, B., Evans, K.A., et al., 2022.
857 Incipient metal and sulfur extraction during melting of metasomatised mantle. Earth
858 Planet. Sci. Lett. 599, 117850, https://doi.org/10.1016/j.epsl.2022.117850.
859 doi:10.1016/j.epsl.2022.117850
860 Rudnick, R. L., McDonough, W. F., Chappell B. W., 1993. Carbonatite metasomatism in

the northern Tanzanian mantle: petrographic and geochemical characteristics. Earth Planet. Sci. Lett. 114, 463-475. doi:10.1093/petroj/39.11-12.1917
Russell, J. K., Kopylova, M. K., 1999. A steady-state conductive geotherm for the north central Slave, Canada: inversion of petrological data from the Jericho kimberlite pipe. J. Geophys. Res. 104, 7089–7101. doi:10.1029/1999JB900012
Russell, J.K., Jones, T.J., 2023. Transport and eruption of mantle xenoliths creates a lagging problem. Comm. Earth Environ. 4, 177. doi:10.1038/s43247-023-00843-0
Scambelluri, M., Vannucci, R., De Stefano, A., Preite-Martinez, M., Rivalenti, G., 2009. CO_2 fluid and silicate glass as monitors of alkali basalt/peridotite interaction in the mantle wedge beneath Gobernador Gregores, Southern Patagonia. Lithos 107, 121-133. doi:10.1016/j.lithos.2008.06.015
Shi, L., Francis, D., Ludden, J., Frederiksen, A., Bostock, M., 1998. Xenolith evidence for lithospheric melting above anomalously hot mantle under the northern Canadian Cordillera. Contrib. Mineral. Petrol. 131, 39-53. doi:10.1007/s004100050377
Sparks, R. S. J., Baker, L., Brown, R.J., Field, M., Schumacher, J., Stripp, G., Walters, A., 2006. Dynamical constraints on kimberlite volcanism. J. Volc. Geotherm. Res., 155, 18-48, doi.org/10.1016/j.jvolgeores.2006.02.010.
Sun, C., Liang, Y., 2013. The importance of crystal chemistry on REE partitioning between mantle minerals (garnet, clinopyroxene, orthopyroxene, and olivine) and basaltic melts. Chem. Geol. 358, 23-36. doi:10.1016/j.chemgeo.2013.08.045
Sun, M., Armstrong, R.L., Maxwell, R.J., 1991. Proterozoic mantle under Quesnellia: variably reset Rb–Sr mineral isochrons in ultramafic nodules carried up in Cenozoic volcanic vents of the southern Omineca Belt. Can. J. Earth Sci. 28, 1239-1253. doi:10.1139/e91-111
Taylor Jr., H. P., Frechen, J., Degens, E. T. 1967. Oxygen and carbon isotope studies of carbonatites from the Laacher See district, West Germany, and the Alnö district, Sweden. Geochim. Cosmochim. Acta 31, 407-430. doi:10.1016/0016-7037(67)90051-8
Van Achterbergh, E., Griffin, W. L., Ryan, C. G., O'Reilly, S. Y., Pearson, N. J., Kivi, K., Doyle B. J., 2002. Subduction signature for quenched carbonatites from the deep lithosphere. Geology 30, 8, 743-746. doi:10.1130/0091-7613(2002)030<0743:SSFQCF>2.0.CO;2
Van der Heyden, P., 1992. A middle Jurassic to early Tertiary Andean-Sierran arc model for the Coast Belt of British Columbia. Tectonics 11, 1, 82-97. doi:10.1029/91TC02183
Warren, J.M., 2016. Global variations in abyssal peridotite compositions. Lithos 248–251, 193-219. doi:10.1016/j.lithos.2015.12.023
Wasylenki, L.E., Baker, M.B., Kent, A.J., Stolper, E.M., 2003. Near-solidus melting of the shallow upper mantle: Partial melting experiments on depleted peridotite. J. Petrol. 44 1163–1191. doi:10.1093/petrology/44.7.1163
Wheeler, J. O., Brookfield, A. J., Gabrielse, H., Monger, J. W. H., Tipper, H. W., Woodsworth, G. J., 1991. Terrane Map of the Canadian Cordillera: Geological Survey of Canada Map 1713A, scale 1:2,000,000. doi:10.4095/133550
Workman, R.K., Hart, S.R., 2005. Major and trace element composition of the depleted MORB mantle (DMM). Earth Planet. Sci. Lett. 231, 53-72.

doi:10.1016/j.epsl.2004.12.005
Yaxley, G. M., Green, D. H., 1994. Experimental demonstration of refractory carbonate bearing eclogite and siliceous melt in the subduction regime. Earth Planet. Sci. Lett. 128, 313-325. doi:10.1016/0012-821X(94)90153-8
Yaxley, G. M., Crawford, A. J., Green D. H., 1991. Evidence for carbonatite metasomatism in spinel peridotite xenoliths from western Victoria, Australia. Earth Planet. Sci. Lett. 107, 305-317. doi:10.1016/0012-821X(91)90078-V
Yaxley, G. M., Green D. H., Kamenetsky, V. 1998. Carbonatite Metasomatism in the Southeastern Australian Lithosphere, J. Petrol. 39, 1917–1930. doi:10.1093/petroj/39.11-12.1917

Figure Captions

Fig. 1. Location of the Mt. Preston mantle xenolith locality within the Canadian Cordillera. (A) Mt. Preston field site (red star) shown in the context of the major tectono-morphologic belts of the Canadian Cordillera (modified from Wheeler et al., 1991). (B) Regional geology of the Mt. Preston field site (red star) is situated south of Eutsuk Lake, approximately 40 km east of the Coast Belt. Thick, grey-shaded line indicates boundary between Intermontane Belt (IB) and Coast Belt (CB) (modified from Diakow et al., 2003).

Fig. 2. Mt. Preston mantle xenolith field locality within basanite dyke. (A) Field photograph showing distribution of mantle xenoliths in the dyke. (B) Detailed view of closely packed mantle xenoliths within the dyke separated by small volumes of basanite melt. (C) Photomicrograph in plane-polarized light (PPL) of basanite showing fresh, unaltered, groundmass mineralogy and volcanic texture. The basanite is aphyric, micro-vesicular and contains a partially digested mantle-derived xenocryst. (D) Scanning electron microscope (SEM) images illustrating primary groundmass mineralogy, and their textural relationships, including olivine (ol), plagioclase (plag), ulvöspinel (ul), and calcite (cc). (E) SEM image of vesicle lined by magmatic calcite (cc) produced by fluid-vapour-deposition from exsolved CO_2-rich fluids (e.g., Naughton, 1975; Hunter et al., 2020).

Fig. 3. Cross-polarized (XPL) and backscattered electron (BSE) images showing the three carbonate (cc) habits found in Mt. Preston mantle xenoliths. (A–C) show carbonate (magnesian calcite) in association with sulphides (cpy: chalcopyrite and pn: pentlandite), with Fe, Ni, and Cu EPMA element maps shown in panel C. (D–E) show intergranular carbonate with olivine (ol), orthopyroxene (opx), and clinopyroxene (cpx). (G–I) show carbonate as an interstitial phase (G) or as inclusions in association with spinel (spl) and cpx (panels H and I).

Fig. 4. Bulk-rock major element proxies of melt depletion from the Mt. Preston mantle xenolith suite and published data for Canadian Cordilleran xenoliths. (A–C) Major elements (TiO_2 wt. %, CaO wt. %, and Al_2O_3 wt. %) *vs*. MgO wt. % for mantle xenoliths (lherzolites, harzburgites, and dunites) from Mt. Preston, Northern Cordilleran Volcanic Province (NCVP; see Francis et al., 2010), and Southern Cordilleran Volcanic Province (SCVP; Peslier et al., 2002). (D) Ca *vs*. Al wt. % in mantle xenoliths from the Canadian Cordillera.

Data sources as in A–C. Blue dashed line with arrows indicates expected trend for depletion of oceanic peridotite (Boyd, 1989).

Fig. 5. Rare earth element (REE) contents of mantle xenoliths. (A) Data normalized to primitive mantle (PM; McDonough and Sun, 1995) for xenoliths from Mt. Preston (solid lines) and other Canadian Cordillera localities (dashed lines; Northern Cordillera, Harder and Russell, 2006; Southern Cordillera, Peslier et al., 2002). (B) Mt. Preston REE data compared to REE fractional melting models (anhydrous) after Warren (2016) using the melting reaction of Wasylenki et al. (2003), partition coefficients from Sun & Liang (2013), and depleted mantle (DM) values from Workman & Hart (2005). Coloured lines are keyed to the mantle equilibration temperatures of each xenolith (side bar). (C) Bulk-rock Tb/Yb *vs.* Al_2O_3 for Canadian Cordillera mantle xenoliths (after Peslier et al., 2002); data sources are as in (A). Coloured symbols are keyed to the mantle equilibration temperatures of xenoliths (side bar). Solid grey lines denote melting trends for spinel and garnet stable mantle assemblages (Bodinier et al., 1988). Chondritic Tb/Yb (McDonough and Sun, 1995) is also shown (black horizontal dashed line) and delineates the chemical effects of metasomatism.

Fig. 6. Isotopic compositions of samples from Mt. Preston and the literature. (A) Carbon and oxygen isotopic compositions for carbonate from Mt. Preston mantle xenoliths, basanite dyke, and wall rocks. Xenoliths define high- and low-carbon groups shown with their respective means and 2σ uncertainty. Also shown are oxygen isotope compositions for the silicate fractions of the dyke. (B) Comparison of Mt. Preston isotopic data to compositions of mantle-xenolith-hosted carbonate from the literature, including New Mexico (Perkins et al., 2006); Sierra Nevada (Ducea et al., 2005); Hungary (Demény et al., 2004); Slave Craton (van Achterbergh et al., 2002); East African Rift (Lee et al., 2000). (C) Strontium isotope composition of carbonate within mantle peridotites, basanite dyke, and wall rock *vs*. oxygen isotope composition. Also shown are bulk rock Sr data for silicate fractions (SF) from the Mt. Preston dyke, Tasse suite of peridotite xenoliths (Polat et al., 2018), and sodic and potassic alkaline olivine basanites from Jacques Lake, Big Timothy Mountain, and West Kettle River (Sun et al., 1991). The field for primary igneous carbonatites (PIC) is from Taylor et al. (1967), Keller and Hoefs (1995), and Barker (1996); the bulk mantle value is from Harmon and Hoefs (1995) and Deines (2002). Analytical uncertainties are generally smaller than symbols.

Fig. 7. Geothermometry results and model geotherm for Mt. Preston mantle xenoliths. (A) Mean equilibration BK90 temperatures for peridotite xenoliths (Supplementary Material Table S5; Brey and Köhler 1990) plotted sequentially in the order they were analyzed with 1σ error bars. Yellow symbols denote plagioclase-bearing peridotite samples. (B) Model steady-state geotherm where mantle xenoliths are plotted according to their pressure-dependent equilibration temperatures (see text). Moho depth is fixed by geophysics (34 ± 3 km; Calkins et al., 2010) and the lithosphere/asthenosphere boundary (LAB) is estimated from V_P/V_S data to be at 50–70 km (Calkins et al., 2010). Also shown are: i) the model adiabat (heavy black line) for a potential temperature of 1300 °C after Katsura et al. (2010), ii) reference solidi curves (heavy green lines) for fertile and carbonated peridotite, and iii) a basanite melt field (light shaded field) delimited by liquidus curves for anhydrous and

hydrous melts. Model mantle lithosphere geotherms terminate against the adiabat at temperatures of 1313–1320 °C) corresponding to depths of 58–72 km.

Fig. 8. Residence (t_r) and heating (t_h) times for mantle xenoliths transported by basanite magma. (A) Times of magma ascent from 40 (2.8 h) and 60 (4.2 h) km depth at velocities of 4 m s^{-1} and the implied residence times (5.5 h and 8.3h) for a 20 cm diameter xenolith due to lagging (Russell and Jones, 2023). (B) Mantle temperature array with depth based on model geotherm (Fig. 7B). (C) Comparison of xenolith residence times (t_r) to times to heat (t_h) two xenoliths (D=10 and 50 cm) to the temperature of the host basanite as a function of sample depth (and temperature). Smaller xenoliths (D=10 cm) are heated to their core regardless of source depth; larger xenoliths (D=50 cm) rise faster than they are heated except when sourced from mantle depths > 50 km. (D) Values of $(t_h - t_r)$ as a function of source depth and xenolith size (see labels). Positive values of $(t_h - t_r)$ are consistent with carbonate survival (green shading) whilst negative values indicate full heating of xenoliths and possible decomposition of xenolith-hosted carbonate (red shading).

Table 1. Radiogenic and stable isotopic data for Mt. Preston (MP-) mantle xenoliths including Sr data for carbonate fractions (CF) in whole rock powders, two-pyroxene equilibration temperatures calculated after Brey and Kohler, (1990; BK90), approximate CO_2 contents via loss on ignition (LOI), and whole rock Al_2O_3 wt. % values (proxy for melt depletion). Values also reported for Sr standards (SRM987) and for replicates[1].

Strontium (± 2σ)

Sample / Description	Rock Type	$^{87}Sr/^{86}Sr$	$^{86}Sr/^{88}Sr$	T (°C)	±1σ	wt. % CO_2	Al_2O_3 wt.%
MP05-159A / (CF)	Lherzolite	0.704618 ± 0.000008	0.1198	863	11	0.33	2.84
MP05-160A / (CF)	Lherzolite	0.704432 ± 0.000008	0.1196	919	9	0.33	4.26
MP05-164A / (CF)	Lherzolite	0.704610 ± 0.000008	0.1196	828	8	0.29	2.91
MP05-164A[1] / (CF)	Lherzolite	0.704607 ± 0.000009	0.1199	"	"	"	"
SRM987 (600 ng)	Standard	0.710220 ± 0.000008	0.1195	–	–	–	–
SRM987 (300 ng)	Standard	0.710233 ± 0.000008	0.1200	–	–	–	–
SRM987 (600 ng)	Standard	0.710232 ± 0.000007	0.1192	–	–	–	–

Carbon and Oxygen (± 1σ)

Sample	Rock Type	$\delta^{13}C$ (‰ vs. VPDB)	$\delta^{18}O$ (‰ vs. VSMOW)	T (°C)	±1σ	wt. % CO_2	Al_2O_3 wt.%
MP05-31	Lherzolite	-4.36 ± 0.10	12.46 ± 0.08	842	4	0.33	2.94
MP05-35	Lherzolite	-5.67 ± 0.06	11.20 ± 0.06	862	13	0.33	2.01
MP05-35[1]	Lherzolite	-6.09 ± 0.04	10.92 ± 0.05	862	13	0.33	2.01
MP05-44	Lherzolite	-5.72 ± 0.04	11.17 ± 0.03	858	8	0.33	2.18
MP05-50	Lherzolite	-5.74 ± 0.07	10.91 ± 0.11	811	19	0.26	2.45
MP05-69	Websterite	<d/l	<d/l	867	20	0.11	11.9
MP05-70A	Lherzolite	-4.41 ± 0.06	11.35 ± 0.06	869	9	0.29	2.77
MP05-78	Lherzolite	-6.03 ± 0.03	12.26 ± 0.05	888	9	0.26	3.43
MP05-79A	Ol-Websterite	-4.20 ± 0.05	11.82 ± 0.05	891	12	0.33	6.27
MP05-139	Lherzolite	-5.75 ± 0.07	11.26 ± 0.09	862	6	0.26	4.71
MP05-159A	Lherzolite	-5.79 ± 0.05	12.35 ± 0.05	863	11	0.33	2.84
MP05-160A	Lherzolite	-3.72 ± 0.04	11.41 ± 0.04	919	9	0.33	4.26
MP05-160B	Dunite	-3.37 ± 0.06	11.64 ± 0.07	1044	7	0.29	0.18
MP05-161D	Harzburgite	-3.51 ± 0.08	10.26 ± 0.09	816	19	0.26	1.36
MP05-162A	Ol-Websterite	-4.19 ± 0.05	11.34 ± 0.04	866	7	0.26	5.75
MP05-164A	Lherzolite	-5.87 ± 0.03	11.30 ± 0.06	828	8	0.29	2.91

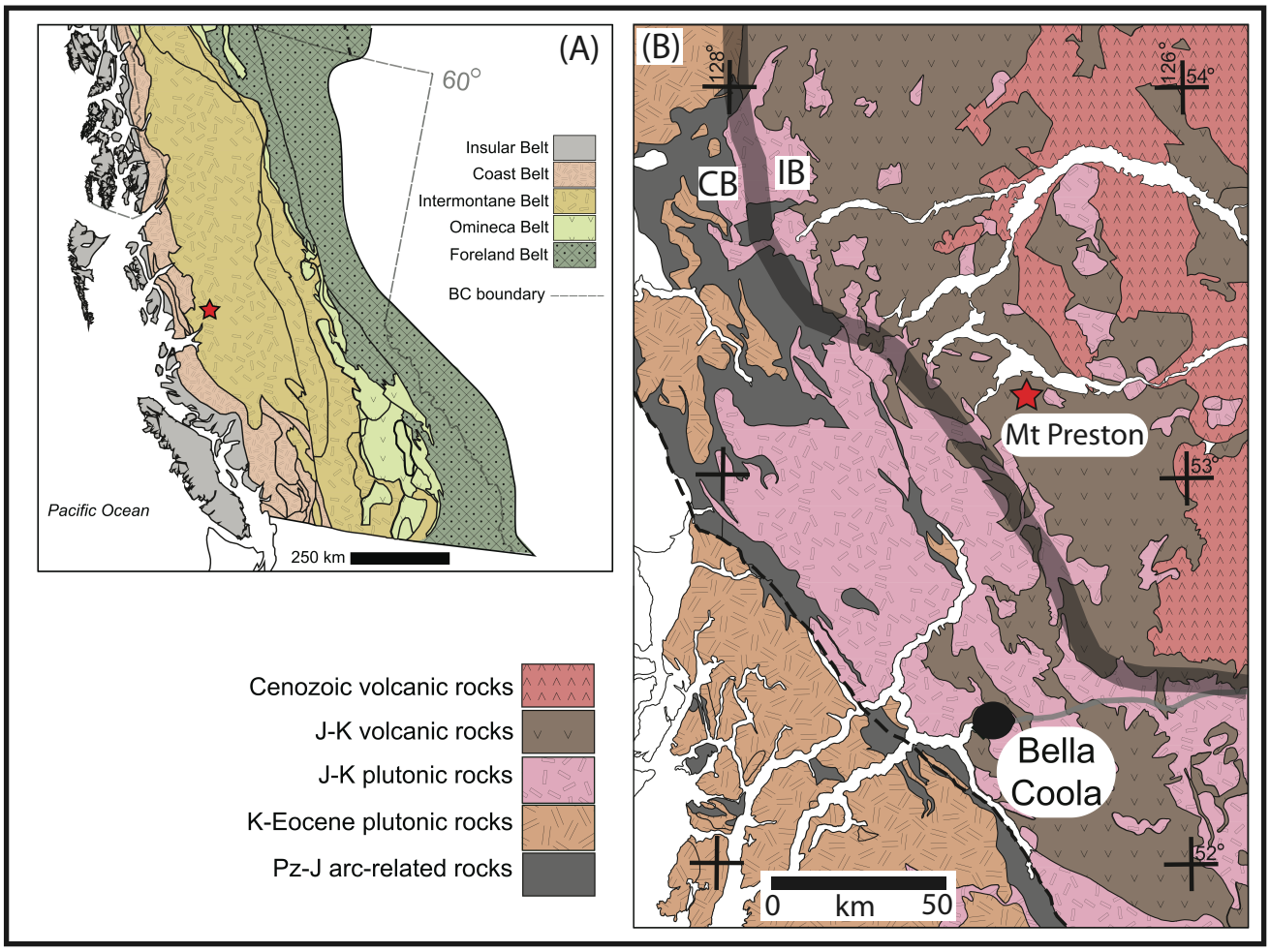

Figure 1. (CJES, Peterson et al. Revised, 2025)

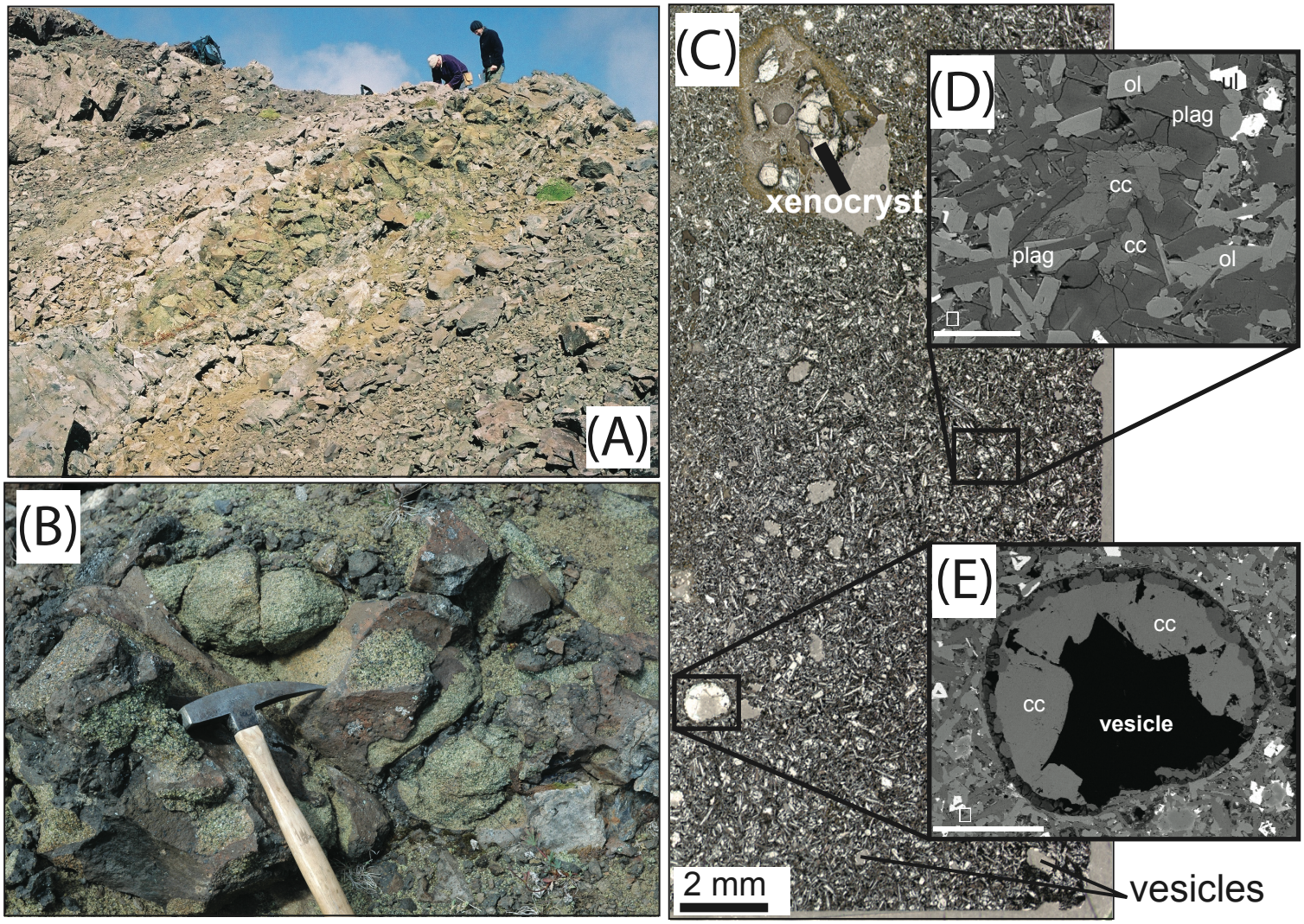

Figure 2. (Peterson et. al, Revised 2025)

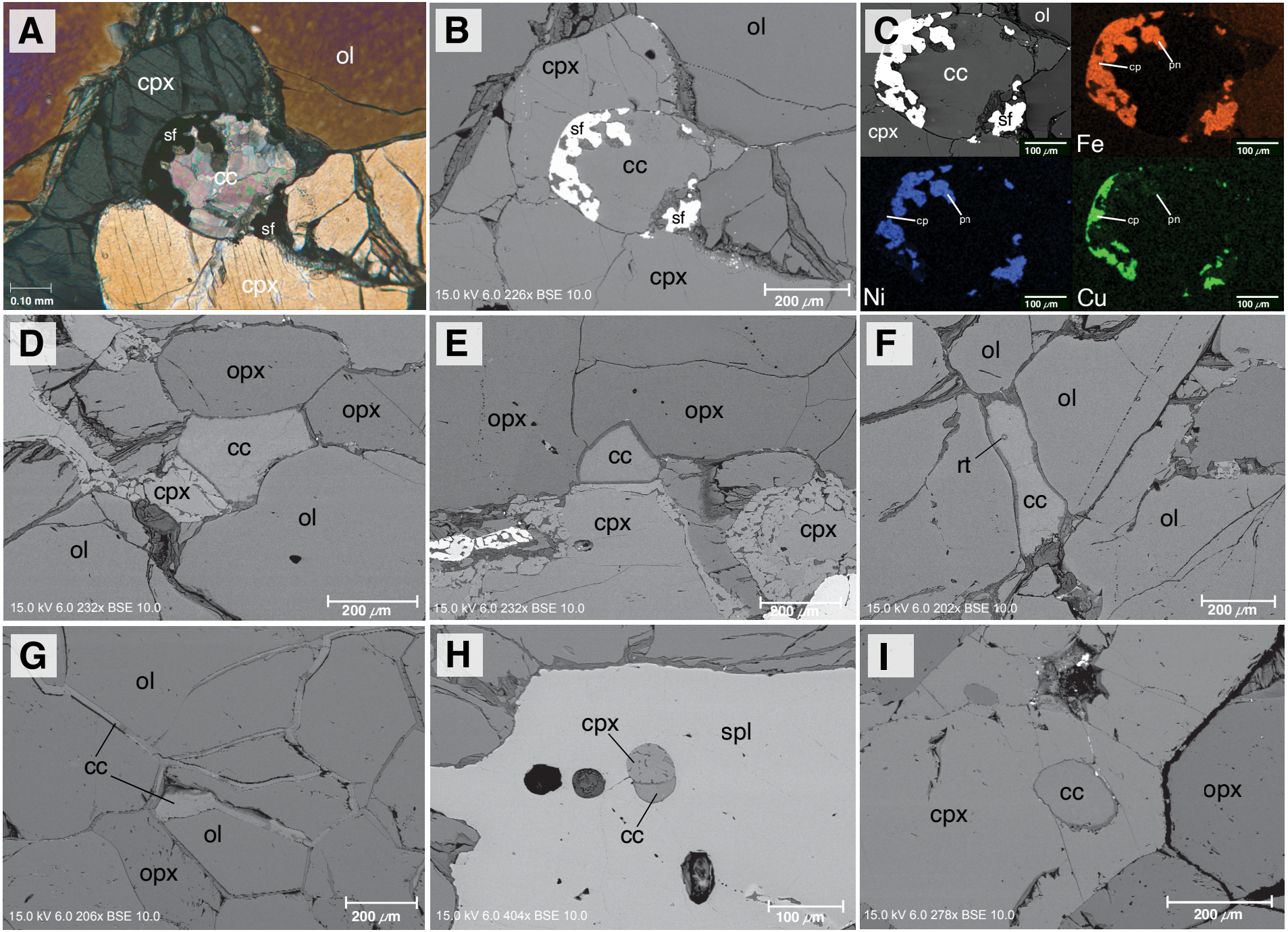

Figure 3. (Peterson et al., Revised 2025)

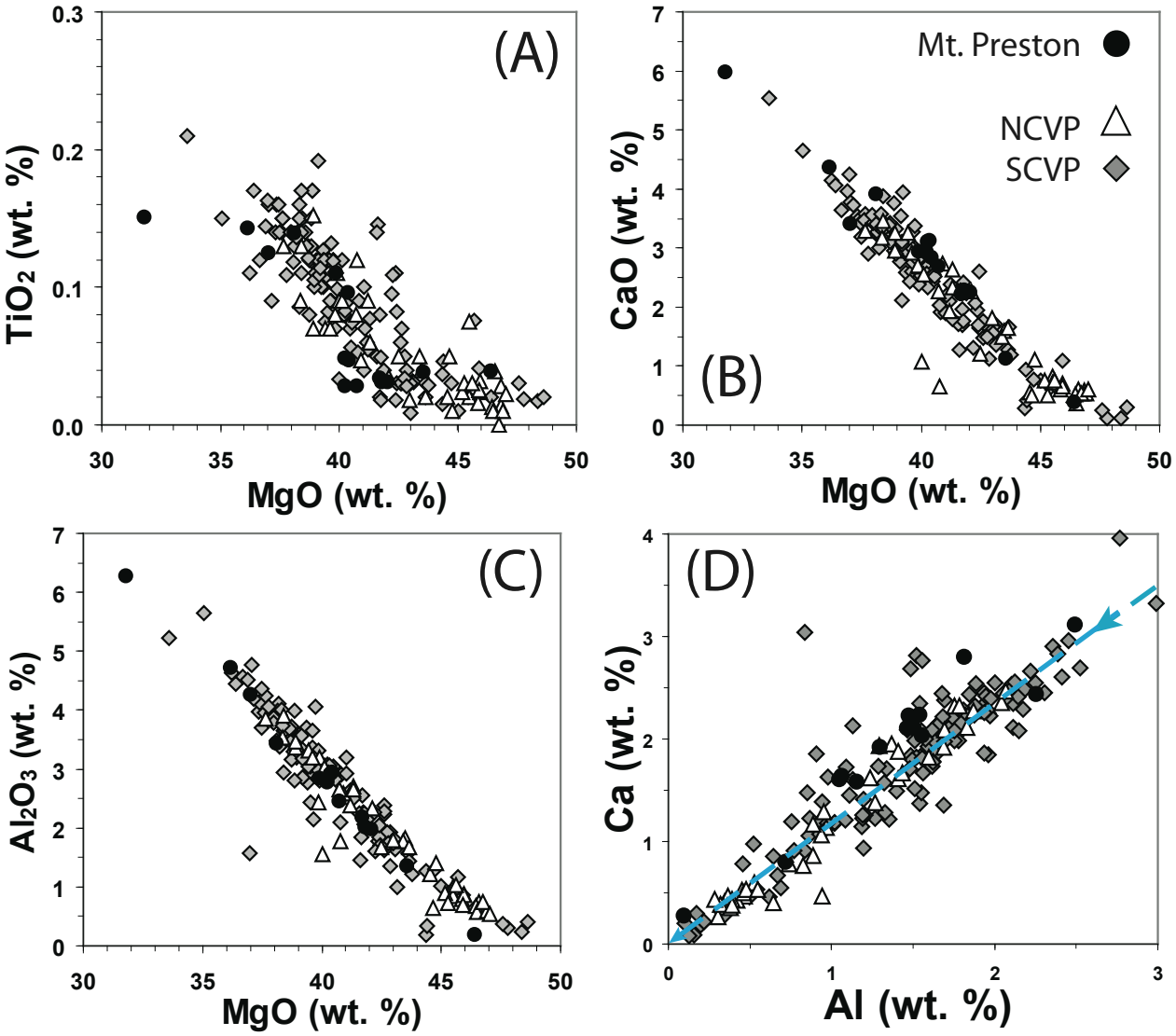

Figure 4. (Peterson et. al, Revised 2025)

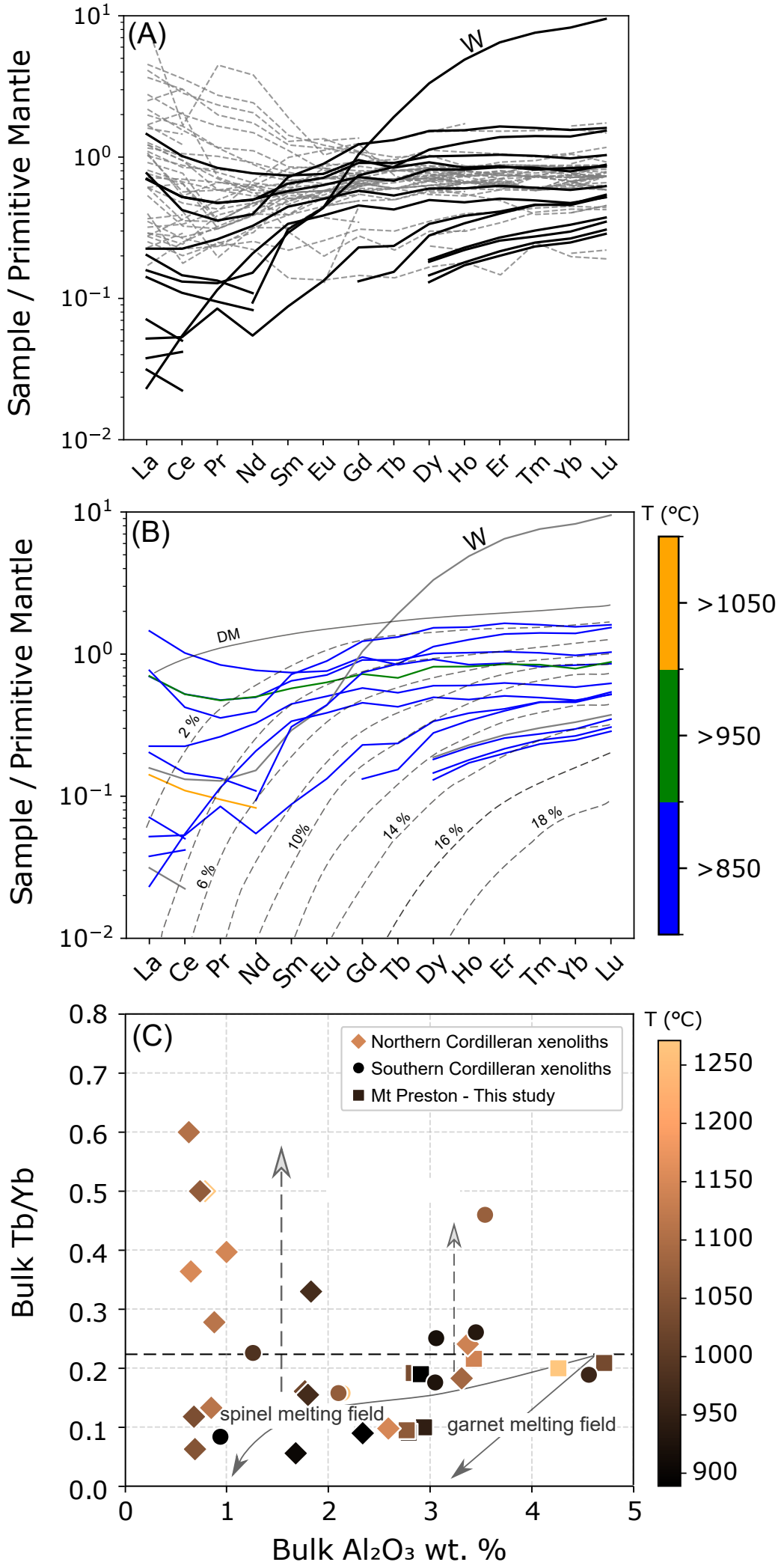

Figure 5. (Peterson et al., Revised 2025)

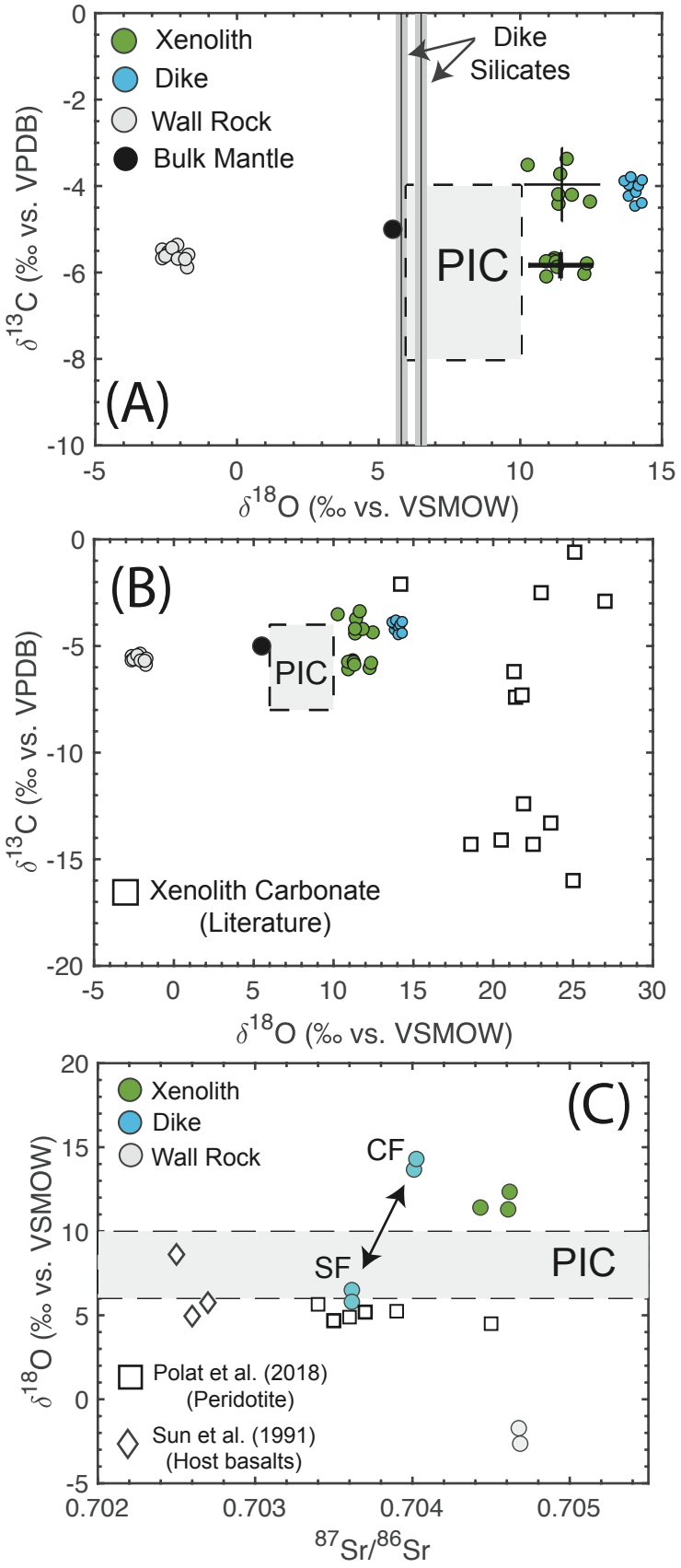

Figure 6. (Peterson et. al, Revised 2025)

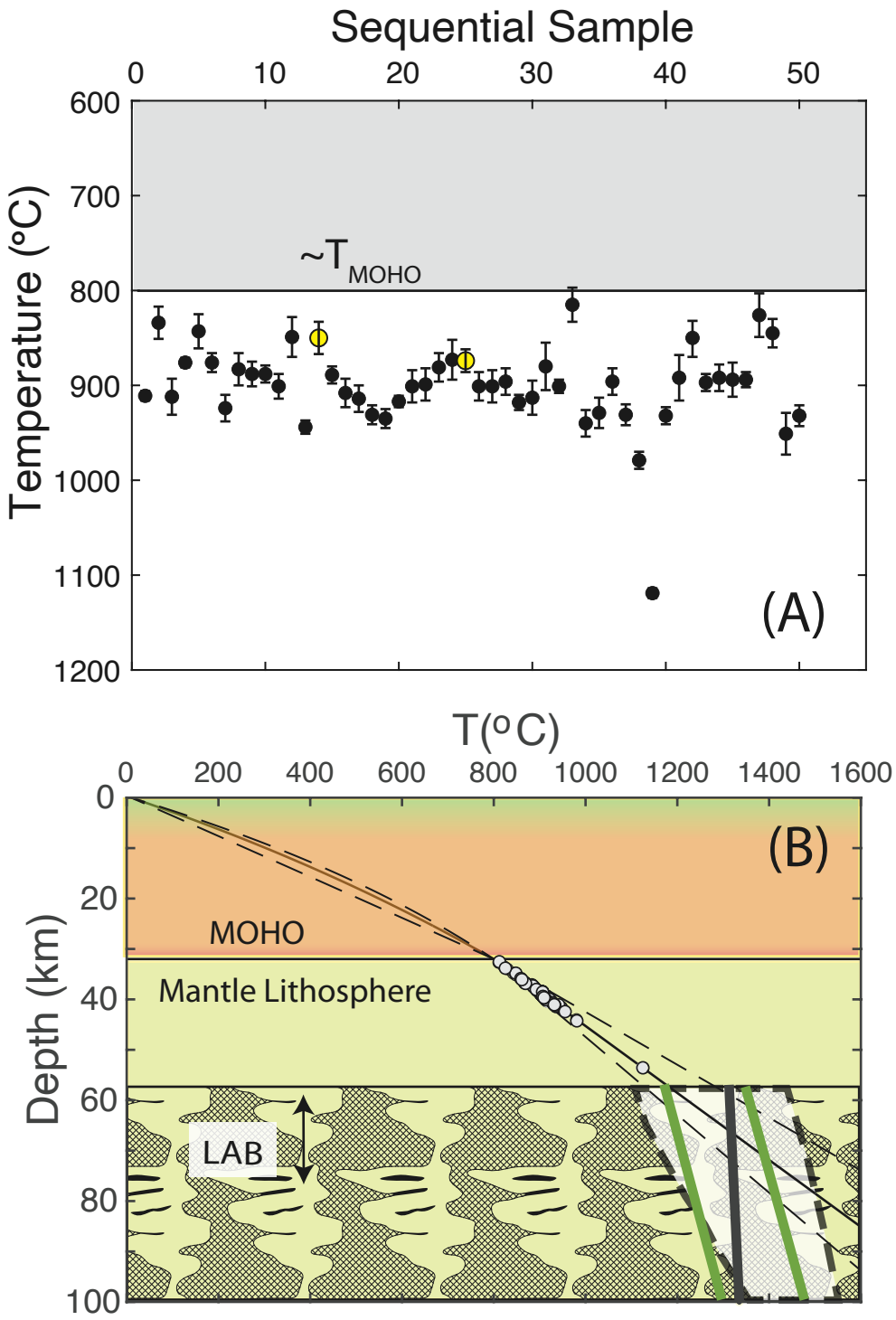

Figure 7. (CJES, Peterson et al. Revised, 2025)

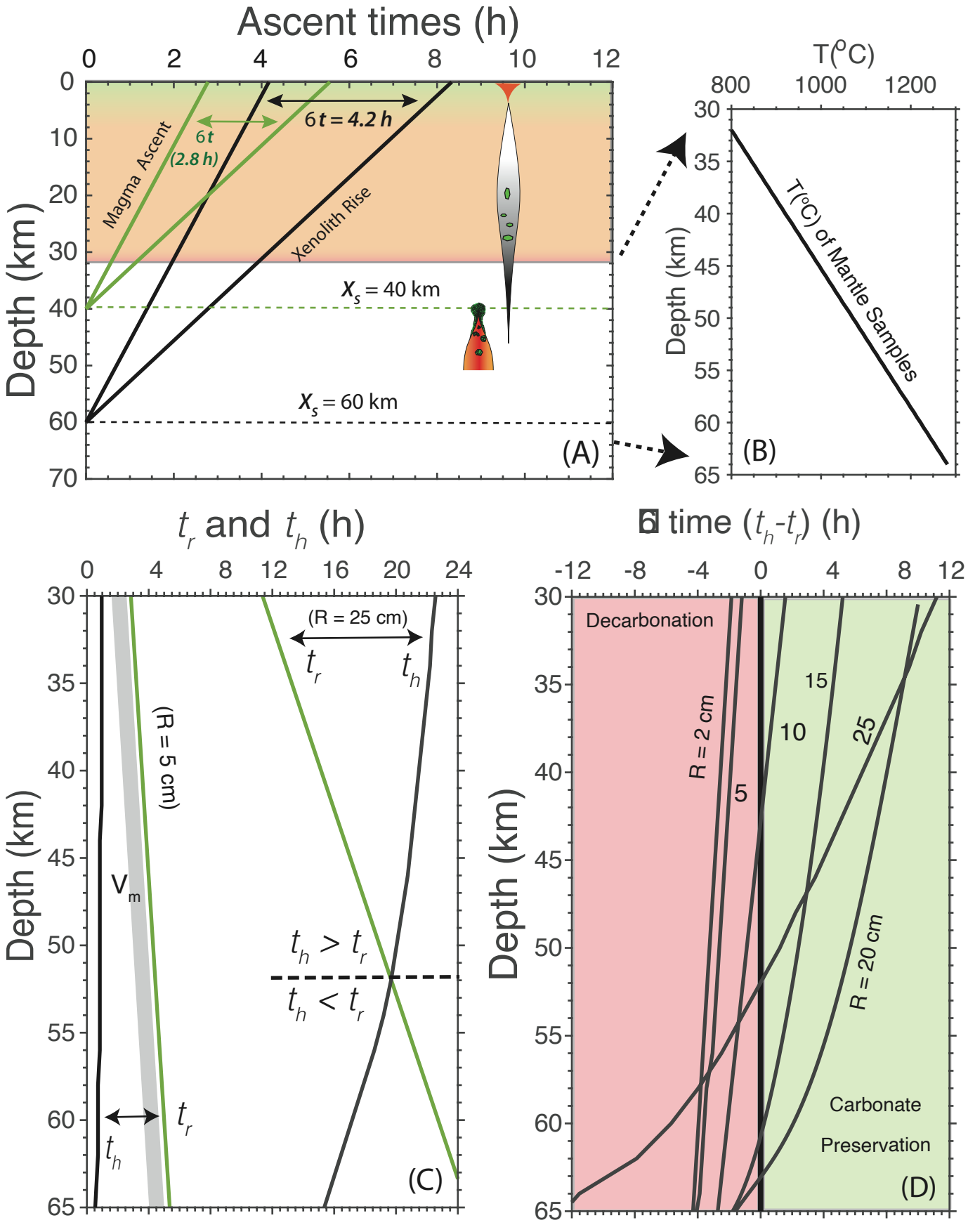

Figure 8 [Peterson et al., revised, 2025]